Author Manuscript

Author Manuscript

Author Manuscript

Author Manuscript

HHS Public Access

Author manuscript

Mol Cell. Author manuscript; available in PMC 2019 March 01.

Published in final edited form as:

Mol Cell. 2018 March 01; 69(5): 879–892.e5. doi:10.1016/j.molcel.2018.01.031.

Histone chaperones ASF1 and CAF-1 promote MMS22L-TONSL-mediated Rad51 loading onto ssDNA during homologous recombination in human cells

Ting-Hsiang Huang[1], **Faith Fowler**[1], **Chin-Chuan Chen**[2], **Zih-Jie Shen**[1], **Barry Sleckman**[1], and **Jessica K. Tyler**

[1]Weill Cornell Medicine, Department of Pathology and Laboratory Medicine, New York, NY 10065, USA

[2]Graduate Institute of Natural Products, Chang Gung University, Taoyuan, 333, Taiwan

Summary

The access-repair-restore model for the role of chromatin in DNA repair infers that chromatin is a mere obstacle to DNA repair. However, here we show that blocking chromatin assembly, via knockdown of the histone chaperones ASF1A, CAF-1 or a mutation that prevents ASF1A binding to histones, hinders Rad51 loading onto ssDNA during homologous recombination. This is a consequence of reduced recruitment of the Rad51 loader MMS22L-TONSL to ssDNA, resulting in persistent RPA foci, extensive DNA end-resection, persistent activation of the ATR-Chk1 pathway and cell cycle arrest. In agreement, histones occupy ssDNA during DNA repair in yeast. We also uncovered DNA-PKcs-dependent DNA damage-induced ASF1A phosphorylation, which enhances chromatin assembly, promoting MMS22L-TONSL recruitment and hence Rad51 loading. We propose that transient assembly of newly-synthesized histones onto ssDNA serves to recruit MMS22L-TONSL to efficiently form the Rad51 nucleofilament for strand invasion, suggesting an active role of chromatin assembly in homologous recombination.

dTOC Blurb

Huang et al. show that the ASF1 and CAF-1 histone chaperones play active roles in DNA double-strand break repair, by promoting the recruitment of MMS22L/TONSL to ssDNA to load Rad51 during homologous recombination in human cells. Furthermore, they show that histones occupy ssDNA during homologous recombination in yeast.

[+]Correspondence: jet2021@med.cornell.edu.
Lead Contact: Jessica Tyler

Publisher's Disclaimer: This is a PDF file of an unedited manuscript that has been accepted for publication. As a service to our customers we are providing this early version of the manuscript. The manuscript will undergo copyediting, typesetting, and review of the resulting proof before it is published in its final citable form. Please note that during the production process errors may be discovered which could affect the content, and all legal disclaimers that apply to the journal pertain.

Author Contributions

JT, T-HH and BS guided the project. FF performed experiments in Fig. 3G and S3A, Z-JS in Fig. 6E-G, C-CC performed the analyses in Fig. 7G and T-HH performed all the remaining experiments. T-HH and JT wrote the manuscript.

Declaration of Interests: The authors declare no competing interests.

Author Manuscript Author Manuscript Author Manuscript Author Manuscript

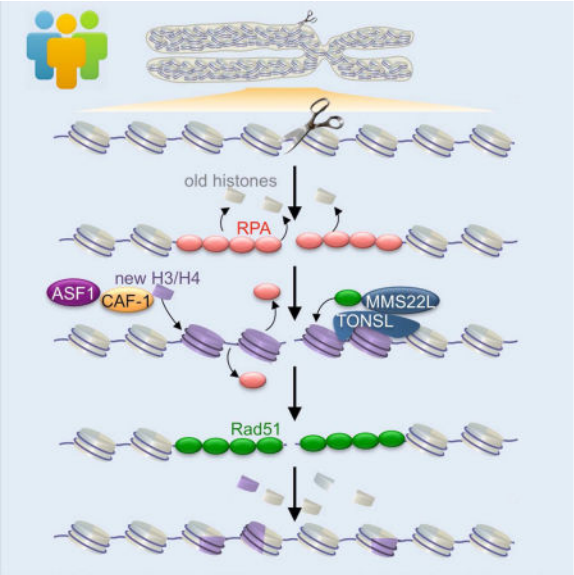

Introduction

DNA double-strand breaks (DSBs) are the most perilous form of DNA lesion, given that they can lead to loss of chromosome arms or cell death if unrepaired. Alternatively, their inaccurate repair leads to chromosomal translocations and mutations, causing diseases such as cancer (Jackson and Bartek, 2009). As a consequence, cells have evolved rapid and efficient mechanisms to respond to DSBs, involving sensing the DNA lesion, amplifying this signal and coordinating the control of the cell cycle via DNA damage checkpoints with DNA repair processes (Ciccia and Elledge, 2010). This is collectively referred to as the DNA damage response (DDR).

One of the key kinase signalling cascades mediating the DDR in mammals is the ataxia telangiectasia and Rad3-related (ATR) - checkpoint kinase 1 (Chk1) pathway (Ciccia and Elledge, 2010). ATR is activated by replication protein A (RPA) bound to stretches of ssDNA that are generated from DNA end-resection during homologous recombinational repair or at stalled replication forks (Marechal and Zou, 2013). Once activated, ATR phosphorylates its transducer kinase Chk1, then ATR and Chk1 phosphorylate many additional proteins to enhance the DDR, DNA repair and to induce cell cycle arrest until the DNA damage has been repaired (Ciccia and Elledge, 2010). DSBs are repaired by two central pathways in eukaryotes: homologous recombination (HR) and non-homologous end joining (NHEJ) (Mehta and Haber, 2014). NHEJ involves the rejoining of DSB ends with little to no end processing and is inherently inaccurate, while HR involves the exchange of a DNA strand of identical sequence from a homologous template via strand invasion, resulting in accurate repair (Chapman et al., 2012). Once DSB repair is complete, ATR and the DNA damage cell cycle checkpoint are inactivated, by unclear mechanisms, to enable cells to resume growth.

Author Manuscript Author Manuscript Author Manuscript Author Manuscript

All DNA repair pathways occur in the context of chromatin within our cells, which is the nucleoprotein structure of arrays of nucleosomes, each of which comprises 147bp of DNA wrapped around the outside of octamers of core histones (Kornberg, 1974). The packaging of DNA into chromatin helps regulate the accuracy and efficiency of the DNA repair process and the DDR in general (Xu and Price, 2011). For example, histone post-translational modifications help recruit proteins involved in the DDR to DSBs (Williamson et al., 2012). Furthermore, histones are removed from around DSBs to enable DNA repair in yeast and human cells (Berkovich et al., 2007; Chen et al., 2008; Goldstein et al., 2013; Li and Tyler, 2016). The requirement for chromatin disassembly for DSB repair implies that histones are a physical obstacle, as described in the access-repair-restore model (Polo and Almouzni, 2015). Intriguingly, “replication-dependent” chromatin assembly by the Asf1 and CAF-1 histone chaperones after DSB repair is required for turning off the DNA damage cell cycle checkpoint in yeast (Chen et al., 2008; Diao et al., 2017; Kim and Haber, 2009). However, whether chromatin assembly plays a role in inactivation of the DNA damage checkpoint after DNA repair in metazoans is unknown.

Consistent with their role in yeast, ASF-1 and CAF-1 have also been shown to mediate chromatin assembly after DSB repair in human cells. So far, this has been shown following NHEJ (Li and Tyler, 2016), but whether they play this same role following HR in humans is unknown. A potential link between the replication-dependent chromatin assembly pathway and homologous recombination was suggested by an interaction between ASF1A and MMS22L-TONSL (Duro et al., 2010). MMS22L-TONSL is recruited to ssDNA coated with RPA to facilitate efficient loading of the strand exchange protein Rad51 onto ssDNA (Duro et al., 2010; O’Donnell et al., 2010)(Piwko et al., 2016), which is an intermediate event in homologous recombination necessary for strand invasion following replication stress or during DSB repair. Noteworthy, recruitment of MMS22L-TONSL to sites of DNA replication is mediated by the interaction between TONSL and newly-synthesized histones that are unmethylated on H4 K20 (Saredi et al., 2016) that are deposited onto DNA by ASF1 and CAF-1.

In this work, we set out to determine if the role of chromatin assembly in inactivation of the DNA damage checkpoint after DSB repair was conserved from yeast to humans. Although we find persistent activation of the ATR-Chk1 pathway upon knockdown of human ASF1 or CAF-1, this was due to a defect in homologous recombination *per se*. Specifically, we find that the replication-dependent histone chaperones ASF1 and CAF-1 promote recruitment of MMS22L-TONSL to facilitate Rad51 loading onto resected DNA. We also have uncovered DSB-induced phosphorylation of ASF1A that promotes these functions. Taken together, these studies reveal an active role for the replication-dependent histone chaperones in the midst of homologous recombination.

Results

Cells lacking ASF1 or CAF-1 have prolonged Chk1 phosphorylation after DSB induction, leading to a delay in cell cycle progression

To determine if chromatin assembly was required for inactivating the DNA damage checkpoint in human cells, we knocked down ASF1A/B, induced DNA damage with the

Author Manuscript Author Manuscript Author Manuscript Author Manuscript

radiomimetic bleomycin, and examined checkpoint activation at increasing times post bleomycin removal (Fig. 1A). In all experiments, the samples that were not exposed to bleomycin "−", were incubated for the same length of time as the longest recovery time post bleomycin removal. Compared to the scrambled sh/siRNA controls, ASF1 depletion with 2 different sets of shRNAs in HeLa or U-2 OS cells (Fig. 1A; S1A) or with siRNA (Fig. 1B) led to persistent ATR-mediated phosphorylation of Chk1 at Ser345 ($Chk1_{S345p}$). Persistent Chk1 phosphorylation in the absence of ASF1 also occurred following treatment with neocarzinostatin (NCS), another radiomimetic drug (Fig. S1B), but not following UV irradiation (Fig. S1C). The persistence of Chk1 activity in the absence of ASF1A/B does not reflect stabilization of the Chk1 protein, because there was no difference in Chk1 protein half-life upon inhibition of translation (Fig. S1D). Knockdown of ASF1B revealed that ASF1A is sufficient to turn off the DNA damage checkpoint after DSB induction (Fig. 1C). In agreement, expression of ASF1A was sufficient to rescue checkpoint inactivation after DSB induction upon ASF1A/B knockdown (Fig. 1D). When ASF1A alone was knocked down, the vast majority of Chk1 was dephosphorylated after DSB induction, although a low proportion of the Chk1 remained persistently phosphorylated (Fig. 1C). As such, there is clearly some redundancy between the function of ASF1A and ASF1B in inactivation of Chk1 after DSB induction, while ASF1A alone is sufficient to inactivate Chk1. Taken together, these data demonstrate that ASF1 is needed for timely ATR-Chk1 inactivation in human cells after DSB induction.

Next, we asked whether the persistent activation of Chk1 in the absence of ASF1 after DSB induction was accompanied by cell cycle arrest. Inducing DSBs in cells depleted for ASF1 led to persistent phosphorylation of Cdk1 on Y15 (Fig. 2A), which prevents premature entry into mitosis (Shaltiel et al., 2015). Furthermore, the persistent phosphorylation of Cdk1 following DSB induction in ASF1 knockdown cells was Chk1 dependent, because it was reduced by addition of Chk1 inhibitor AZD7762 (Fig. 2B). In agreement with the persistent phosphorylation of Cdk1, DSB induction caused cells depleted of ASF1 to accumulate with a G_2/M phase DNA content (Fig. 2C), consistent with cell cycle arrest.

ASF1 is the upstream histone chaperone for replication-independent chromatin assembly of histones H3.3/H4 by the HIRA histone chaperone, and for replication-dependent chromatin assembly of histones H3.1/H4 by CAF-1 (Hammond et al., 2017). To determine whether either of these chromatin assembly pathways are required for efficient inactivation of the ATR-Chk1 pathway after DSB induction, we knocked down HIRA and CAF-1. Knockdown of the large subunit of CAF-1, CAF-1 p150, but not HIRA, led to persistent Chk1 phosphorylation and persistent Cdk1 phosphorylation following DSB induction (Fig. 2D, E). These data indicate that only the replication-dependent chromatin assembly pathway promotes checkpoint inactivation after DSB induction in humans, reminiscent of the situation in yeast (Chen et al., 2008; Kim and Haber, 2009).

The replication-dependent chromatin assembly pathway promotes the transition from RPA-coated ssDNA to Rad51-coated ssDNA during homologous recombination

The persistent activation of Chk1 that occurs upon ASF1 and CAF-1 knockdown following DSB induction led us to ask if this is accompanied by persistent activation of the ATR

Author Manuscript Author Manuscript Author Manuscript Author Manuscript

kinase. By examining the kinetics of accumulation and dissipation of ATR at DNA repair foci, we observed persistent accumulation of ATR upon knockdown of ASF1, as compared to the control (Fig. 3A). Consistent with ATR activation by RPA bound to ssDNA, we also observed persistent retention of RPA at DNA repair foci at increasing after DSB induction upon ASF1 knockdown, as compared to the control (Fig. 3A). Phosphorylation of RPA bound to ssDNA on Ser4/Ser8 is important for full ATR activation (Liu et al., 2012). Consistent with there being persistent DSBs resected to ssDNA in cells depleted of ASF1A/B, we saw persistent Ser4/Ser8 phosphorylation on RPA2 ($RPA_{S4/S8}$) in both HeLa and U-2 OS cells (Fig. 3B, Fig. S1A), but only after inducing DSBs. While the persistent Chk1 phosphorylation seen in ASF1 depleted cells after DSB damage was blocked by the ATR inhibitor, VE-821, this was not the case with the $RPA2_{S4/S8}$ phosphorylation (Fig. S2), consistent with it being mediated by DNA-PKcs. Persistently activated RPA2 was also observed upon CAF-1 knockdown, but not upon HIRA knockdown (Fig. 3C), indicating that the replication-dependent chromatin assembly pathway was required for terminating hyperactivated RPA.

To understand the mechanism behind the prolonged ATR-RPA2-Chk1 signalling upon defective replication-dependent chromatin assembly, we asked if there was more ssDNA present after DSB induction in ASF1 depleted cells. We used native BrdU immunofluorescence staining to detect BrdU in ssDNA, but not within dsDNA (Raderschall et al., 1999) after exposure of cells to camptothecin or bleomycin. Camptothecin is a topoisomerase I poison that induces DSBs during replication. The amount of BrdU at ssDNA upon depletion of ASF1 was significantly higher than in the control cells following camptothecin (Fig. 3D) or bleomycin treatment (Fig. 3E). As a control for reduced or increased end resection during DSB repair, we knocked down the exonuclease CtIP or 53BP1, respectively. Noteworthy, the amount of end resection observed upon ASF1 knockdown was comparable to the extreme amount of resection that occurs upon 53BP1 knockdown (Fig. 3E). These results suggest that ASF1 plays a role in protecting DSB ends from excessive resection.

During the process of homologous recombination, RPA is displaced from ssDNA by an unclear mechanism, and is replaced by Rad51 to form the nucleofilament that initiates strand invasion. Given that there was persistent RPA foci formation following DSB induction in ASF1 depleted cells, we asked if this was accompanied by reduced Rad51 nucleofilament formation. Indeed, we observed a significant reduction in the number of cells with Rad51 foci after DSB induction in ASF1 depleted cells (Fig. 3F). Reduced Rad51 loading onto ssDNA in the ASF1 depleted cells was not an indirect consequence of reduced levels of total Rad51, because Rad51 protein levels were unaffected by ASF1 knockdown (Fig. S3A). To validate the extensive end resection observed upon ASF1 depletion and to compare its effect to loss of Rad51, we used a more quantitative assay to measure end resection at increasing distances from a tamoxifen-inducible AsiSI cut site (Zhou et al., 2014). We reasoned that reduced Rad51 loading onto ssDNA would lead to more extensive end resection following DSB induction. Indeed, knockdown of ASF1 or RAD51 significantly increased DNA end resection (Fig. 3G, S3B). These data show that ASF1 promotes Rad51 loading during HR, and in its absence, excessive end resection and persistent checkpoint activation occurs.

Author Manuscript Author Manuscript Author Manuscript Author Manuscript

ASF1 and CAF-1 promote recruitment of MMS22L-TONSL to chromatin to load Rad51 during HR

Towards understanding the mechanism whereby ASF1 promotes Rad51 loading during HR, we were intrigued by the physical interaction between ASF1A/B and the Rad51 loader MMS22L-TONSL (Duro et al., 2010). Reminiscent of what we observed with cells depleted of ASF1 or CAF-1, MM22L and TONSL depletion with two different shRNAs led to persistent phosphorylation of $Chk1_{S345}$, $RPA2_{S4/S8}$ and $Cdk1_{Y15}$ following removal of bleomycin in both HeLa and U-2 OS cells (Fig. 4A, 4B, S4A), suggesting that MMS22L, TONSL, ASF1 and CAF-1 might be functioning in the same pathway during HR. Using chromatin fractionation, MMS22L depletion did not have a significant effect on recruitment of either CAF-1 or ASF1 to chromatin (Fig. S4B). Noteworthy, MMS22L depletion drastically reduced the total amount of TONSL protein in human cells and vice versa, consistent with them stabilizing each other (Fig. 4C, S4A, S4C). Conversely, MMS22L-TONSL recruitment to chromatin was enhanced by the replication-dependent chromatin assembly pathway because knockdown of CAF-1 or ASF1, but not HIRA, reduced MMS22L-TONSL levels on chromatin (Fig. 4C). This was also the case following DSB induction (Fig. S4C). Furthermore, the recruitment of MMS22L to DNA damage foci after DSB induction was dependent on ASF1 and CAF-1 (Fig. 4D, 4E). As is the case with ASF1 depletion, CAF-1 or MMS22L depletion, but not HIRA depletion, led to less Rad51 foci after removal of bleomycin in both HeLa and U-2 OS cells using two different shRNAs (Fig. 5A, 5B, S5A). Knockdown of ASF1A/B, CAF-1 and HIRA led to varying degrees of accumulation of cells with an increased G_1/S DNA content (Fig. 5A), as seen previously (Adam et al., 2013; Groth et al., 2005; Hoek and Stillman, 2003), while MMS22L depletion led to accumulation of cells in G_2/M phase, (Fig. 5A), as seen previously (O'Donnell et al., 2010; Piwko et al., 2010). Importantly, the reduced recruitment of Rad51 to DNA repair foci upon depletion of ASF1 or CAF-1 following DSB induction was not due to cells accumulating in G_1/S-phase, because elevated levels of Rad51 foci were not seen upon treatment with aphidicolin alone, which inhibits DNA replication and causes S-phase arrest (Fig. 5A, 5B). Taken together, these data indicate that replication-dependent histone chaperones are required for the recruitment of MMS22L-TONSL during HR to load Rad51 onto ssDNA.

Next, we determined whether ASF1 and CAF-1 are required for DSB repair. We performed comet assays using camptothecin treatment which enriches for DSBs that are repaired by HR. Following camptothecin treatment, cells depleted of ASF1, CAF-1, MMS22L or Rad51 all had long tail moments that were not statistically different from each other, but were significantly longer than the control, suggesting that loss of ASF1, CAF-1, MMS22L or Rad51 cause a similar degree of defect in HR (Fig. 5C,D). To ensure that we were specifically measuring HR, we used a chromosomally integrated DR-GFP reporter in U-2 OS cells that allows homologous gene conversion induced by the I-SceI nuclease (Pierce et al., 1999). We found that depletion of ASF1, CAF-1 or MMS22L led to a similar degree of reduction in HR (Fig. 5E, S5B, S5C). Combined knockdown of ASF1 and CAF-1, or ASF1 and MMS22L reduced HR even further (Fig. 5E), which likely reflects their incomplete knockdown (Fig. S5B). Taken together, these results suggest that MMS22L and the H3.1/H4

Author Manuscript Author Manuscript Author Manuscript Author Manuscript

chaperones promote Rad51 loading onto resected DNA during HR, via ASF1 and CAF-1 promoting MMS22L-TONSL recruitment to chromatin.

ASF1A is phosphorylated on serine 192 in a manner dependent on DNA-PKcs in response to DSBs

During the course of our analyses, we consistently observed a slower migrating form of ASF1A appearing rapidly, in a dose responsive manner, after bleomycin or doxorubicin treatment (Fig. 6A, S6A). This represents phosphorylated ASF1A, because the slower migrating form was abolished by treatment with phosphatase (Fig. 6B). Because ASF1A is known to be phosphorylated by Tousled-like kinases (Tlks) during DNA replication (Mello et al., 2002) on serine 166, 175, 192 and 199 (Klimovskaia et al., 2014), we examined whether mutation of each serine to alanine could block damage-induced ASF1A phosphorylation. Indeed, ASF1A S192A blocked its ability to be phosphorylated in response to DNA damage (Fig. 6C), indicating that $ASF1A_{S192}$ is phosphorylated after DSB induction.

Tlks are specifically inhibited by ATM in response to DNA damage (Groth et al., 2003), suggesting that DSB-induced phosphorylation of ASF1A is not Tlk-dependent. In agreement, ASF1A phosphorylation occurs concomitant with the damage-induced loss of phosphorylation of Tlks substrate Rad9 S328 (Fig. S6B) (Sunavala-Dossabhoy and De Benedetti, 2009). Furthermore, knockdown of TLK1 and 2 resulted in loss of phosphorylation of its substrate Rad9, but had no effect on damage-induced ASF1A phosphorylation (Fig. 6D). Because ASF1A phosphorylation occurs when cells encounter genomic insults, we tested whether the known DNA damage response kinases were responsible. Knockdown or inhibition of ATM or ATR (Fig. 6E, S6C, SCD), or knockdown of Chk1 or Chk2 (Fig. 6F,G) failed to reduce DSB-induced ASF1A phosphorylation. By contrast, inhibition or knockdown of DNA-PKcs greatly reduced or blocked DSB-induced ASF1A phosphorylation (Fig. 6H, I). Inactivation of DNA-PKcs was apparent by the reduced phosphorylation of its substrate $RPA2_{S4/S8}$ and reduced ATR-dependent phosphorylation of Chk1, which is also indirectly promoted by DNA-PKcs (Lin et al., 2014). Furthermore, DSB-induced phosphorylation of ASF1A did not occur in the DNA-PKcs deficient cell line M059J (Fig. S6E). To investigate the function of DSB-induced ASF1A phosphorylation, we observed that phosphorylated ASF1A was enriched on chromatin during DSB induction, followed by increased retention of unphosphorylated ASF1A on chromatin for hours after damage (Fig. 6J). By contrast, in the presence of a DNA-PK inhibitor, the recruitment of phosphorylated ASF1A to chromatin after damage did not occur, nor was ASF1A retained after damage (Fig. 6J). Taken together, these data show that ASF1A is rapidly phosphorylated after DSB induction, in a manner dependent on DNA-PKcs, leading to its enrichment/recruitment to chromatin.

ASF1A phosphorylation facilitates its chromatin localization and histone binding affinity

We examined the potential function of damage-induced ASF1A phosphorylation by mutating serine 192 to aspartic acid to mimic permanent phosphorylation. Chromatin fractionation of cellular extracts shows that ASF1 was recruited to chromatin, and this depended on its ability to bind to histones H3/H4 because the $ASF1A^{V94R}$ mutant, which

Author Manuscript Author Manuscript Author Manuscript Author Manuscript

loses histone binding ability (Mousson et al., 2005), did not interact with chromatin (Fig. 7A). While comparable levels of ASF1A^{WT} and ASF1A^{S192A} were bound to chromatin, ASF1A^{S192D} showed greater binding to chromatin (Fig. 7A), consistent with the idea that DSB-induced ASF1A phosphorylation promotes ASF1A recruitment to chromatin. When cells were pre-extracted with Triton-X to remove soluble ASF1A followed by immunofluorescence analysis, 44.6% of the cells had significant ASF1A^{S192D} retention on the chromatin, as compared to 26 or 29.5% for ASF1A^{WT} and ASF1A^{S192A} respectively (Fig. 7B). Given that the non-histone binding ASF1A^{V94R} mutant was maintained on chromatin in only about 0.5% of cells, chromatin association of ASF1A is likely to reflect its role in chromatin assembly. As such, it appears that the phosphomimetic of ASF1A is likely to promote chromatin assembly. Consistent with ASF1A$_{S192}$ phosphorylation promoting replication-dependent chromatin assembly, ASF1A^{S192D} had enhanced interactions with histone H3.1, H4, and CAF-1 by immunoprecipitation analysis, in comparison to ASF1A^{WT} and ASF1A^{S192A} (Fig. 7C). Furthermore, ASF1A^{S192D} also promoted interaction with MMS22L (Fig. 7C). ASF1A^{S192D} also slightly increased interaction with H3.3, the replication-independent histone variant (Fig. S7). Consistent with the idea that ASF1-mediated chromatin assembly and MMS22L recruitment to DSBs occurs in a manner dependent on ASF1A phosphorylation, we observed an increase in the amount of histones and MMS22L bound to wild type ASF1A after DSB induction, but this did not occur in the ASF1A^{S192A} mutant (Fig. 7D). Taken together, these results suggest that DSB-induced ASF1A phosphorylation promotes chromatin assembly during DSB repair and MMS22L interaction.

Damage-induced ASF1 phosphorylation facilitates Rad51 loading onto ssDNA

Given that DSB-induced phosphorylation of ASF1A enhances ASF1A's interactions with chromatin, histones and MMS22L (Fig. 7C,D), we asked whether ASF1A phosphorylation promoted the MMS22L-TONSL-mediated recruitment of Rad51 during HR. Rad51 recruitment was significantly reduced in cells depleted of endogenous ASF1 that expressed the ASF1A^{V94R} mutant unable to assemble chromatin (Fig. 7E). Furthermore, the ASF1A^{S192A} mutant was as defective at Rad51 recruitment as the ASF1A^{V94R} (Fig. 7E). Given that MMS22L-TONSL is recruited to ssDNA (O'Donnell et al., 2010) and that TONSL is recruited to DSBs via interaction between the TONSL ARD domain and unmethylated H4K20 on newly-synthesized histones (Saredi et al., 2016), we propose a model whereby DNA damage-induced ASF1A phosphorylation promotes replication-dependent chromatin assembly of newly-synthesized histones onto ssDNA, to achieve MMS22L-TONSL recruitment and subsequent Rad51 loading during HR (Fig. 7F).

Histones occupy end resected DNA in budding yeast

Implicit to our model is the presence of histones on the ssDNA generated by end resection during HR. Unfortunately in metazoan cells, end resection occurs too infrequently to experimentally differentiate between histones on ssDNA vs dsDNA. However, induction of a DSB at an HO endonuclease site in a budding yeast strain (JKM179) with no donor sequences is a well-established approach to achieve synchronous and efficient end resection during HR (Eapen et al., 2012). Using real-time PCR to quantitate amplicons at increasing distances from the HO site, at increasing times after HO induction, resection was apparent

Author Manuscript Author Manuscript Author Manuscript Author Manuscript

by reduction in the amount of PCR product (Fig. 7G). Resection removes only one strand of the PCR template, such that the signal was reduced to about half of the initial amplification, although with more time, further loss of signal can be seen in the input DNA to the histone H3 ChIP due to loss of both strands of DNA around the lesion, as seen previously (Eapen et al., 2012). When examining the H3 ChIP signal without normalizing to input, the amount of DNA associated with H3 follows a very similar pattern to the input, albeit with more DNA loss in the H3 ChIP closer to the HO lesion where both strands of the DNA have been lost from the input (Fig. 7G). This result indicates that histones occupy the end-resected DNA, while histones are only lost from the regions closest to the DNA break where both strands of DNA are lost. Indeed when the H3 ChIP signal was normalized to the input, the fold enrichment of the histones was constant regardless of whether the DNA was ssDNA or dsDNA (Fig. 7G). These data indicate that histones are present on ssDNA during HR in yeast. Taken together, this study suggests that histones on ssDNA play an unprecedented active role in promoting DSB repair.

Discussion

In this study, we have unveiled an intrinsic role for replication-dependent chromatin assembly factors in the fundamental mechanism of HR. Our work suggests that chromatin assembly may occur on the ssDNA that results from end resection of DSBs, where the newly-synthesized, unmethylated histones deposited onto the ssDNA function to recruit MMS22L-TONSL to replace RPA with Rad51, in order to form the nucleofilament that mediates strand invasion (Fig. 7F). Furthermore, this function is promoted by DNA-PKcs-dependent ASF1A phosphorylation in response to DSBs. Our results suggest that dynamic chromatin assembly plays an active role in the DNA repair process *per se*.

MMS22L-TONSL is likely to function in the same pathway as replication-dependent chromatin assembly to achieve Rad51 loading onto ssDNA. This is suggested by the observation that ASF1 and CAF-1 are required for recruitment of MMS22L-TONSL to chromatin and DNA repair foci (Fig. 4C-E). Noteworthy, the extent of the HR defect observed for ASF1 or CAF-1 knockdown was similar to that for MMS22L knockdown, using the ISceI HR reporter system (Fig. 5E). Indeed, the DNA damage repair defects for Rad51, MMS22L, TONSL, CAF-1 and ASF1 knockdown were indistinguishable by comet assay (Fig. 5C,D). In agreement, MMS22L, ASF1 and CAF-1 knockdown all led to the same degree of persistent activation of the ATR-RPA-Chk1 pathway and cell cycle arrest after DSB induction (Figs. 1–4). MMS22L, ASF1, or CAF-1 knockdown, or ASF1 mutants that cannot be phosphorylated by DNA-PKcs or bind histones, all resulted in a similar defect in Rad51 loading (Fig. 5B, 7E). Furthermore, ASF1 and CAF-1 function upstream of MMS22L-TONSL in the Rad51 loading pathway, given that ASF1 and CAF-1 are required for recruitment of MMS22L-TONSL to chromatin and DNA repair foci. It is possible however, that MMS22L-TONSL, ASF1 or CAF-1 may play additional unique roles in homologous recombination (Fig. 5E).

Author Manuscript Author Manuscript Author Manuscript Author Manuscript

Replication-dependent chromatin assembly factors promote Rad51 recruitment to ssDNA and limit end resection

We propose that ASF1 and CAF-1 assemble chromatin onto ssDNA rather than dsDNA during HR (Fig. 7F) for the following reasons. The evidence that MMS22L-TONSL is recruited to RPA-bound ssDNA produced from DSB processing is compelling (Piwko et al., 2016), as is the evidence that MMS22L-TONSL is recruited to DSBs via an interaction with newly-synthesized histones (Saredi et al., 2016). Our work synthesizes these observations to suggest that chromatin is assembled transiently onto RPA-bound ssDNA to recruit MMS22L-TONSL to facilitate homologous recombination. Previous analyses from the Durocher laboratory (O'Donnell et al., 2010) observed a near perfect accumulation of MMS22L and TONSL at sites of DNA damage marked by RPA, contained within γH2AX-marked domains. These RPA containing subchromatin microcompartments have been shown previously to be delineated by ssDNA (Bekker-Jensen et al., 2006), indicating that MMS22L-TONSL colocalize with ssDNA formed following DSB processing. Indeed, depletion of CtIP, a protein that plays a key role in end resection (Sartori et al., 2007), profoundly reduced MMS22L-TONSL recruitment to sites of DNA damage (O'Donnell et al., 2010). Furthermore, a recent study showed that MMS22L, which binds directly to Rad51, is recruited to ssDNA bound by RPA (Piwko et al., 2016). Given that TONSL serves as a reader of H4K20me0 (Saredi et al., 2016), which occurs only transiently on newly-synthesized histones after their assembly onto DNA by ASF1 and CAF-1, our observed requirement for ASF1 and CAF-1 for recruitment of MMS22L-TONSL to ssDNA is consistent with chromatin assembly occurring onto ssDNA following DNA resection. However, new technologies will need to be developed in order to directly demonstrate that chromatin assembly occurs on ssDNA in mammalian cells. Such technologies should enable future experiments to determine whether the ability of ASF1 and CAF-1 to promote HR is indeed through assembly of chromatin onto ssDNA in mammalian cells, and whether histones are assembled into nucleosome-like structures on ssDNA.

Several previous studies support the ability of nucleosomes to assemble onto ssDNA *in vitro*. Nearly 40 years ago, Bruce Alberts reconstituted nucleosomes onto ssDNA that resembled nucleosomes on dsDNA by electron microscopy (Palter et al., 1979). More recently, DNA resection was shown to be able to occur *in vitro* on reconstituted nucleosomal templates, and that histones remain associated with the ssDNA after DNA end resection (Adkins et al., 2017). In agreement, we extend these observations *in vivo* to show that histones occupy end-resected ssDNA with the same level of occupancy as on dsDNA in budding yeast (Fig. 7G). We propose that nucleosomes assembled onto resected ssDNA serves as a platform to specifically recruit DNA repair machineries, such as MMS22L-TONSL. Strikingly, we observed extensive end processing of DSBs into ssDNA in ASF1-depleted cells, equivalent to the levels in cells depleted of 53BP1 (Fig. 3D,E,G). The resection that we observed was strictly dependent on induction of DSBs and is therefore distinct from the increase in ssDNA that has been reported previously in the absence of ASF1 during DNA replication (Groth et al., 2007). Given that we also found an equivalent degree of extensive end resection upon Rad51 depletion (Fig. 3G), these data are consistent with recently assembled chromatin promoting Rad51 loading onto ssDNA and demonstrate

Author Manuscript Author Manuscript Author Manuscript Author Manuscript

that Rad51 functions to limit end resection. Noteworthy, MMS22L knockdown also leads to a similar degree of extensive DNA end resection (O'Donnell et al., 2010).

The role of ASF1 and CAF-1 in promoting HR may also be related to the histone modifications that occur on newly-synthesized histones, given that CAF-1 only assembles newly-synthesized histones onto DNA. In line with this notion, p150 CAF-1 has been shown to promote laser-induced Rad51 nucleofilament formation by transiently recruiting HP1 (Baldeyron et al., 2011) which preferentially binds H3K9me3. Intriguingly, CAF-1 promotes H3K9 methylation on free histones prior to their being deposited onto DNA (Loyola et al., 2006; Sarraf and Stancheva, 2004), raising the possibility that another reason for the dynamic assembly of chromatin during HR may be to establish H3K9me3 at break sites to promote HR. In agreement, depletion of CAF-1 in different species also compromises HR repair (Lewis et al., 2005; Song et al., 2007). We propose that local assembly of unmodified newly-synthesized histones facilitates the recruitment of specific repair factors, such as MMS22L-TONSL, and seemingly HP1, at exactly the time that they are needed to bring Rad51 onto the ssDNA coated with RPA (Fig. 7F). It is possible that RPA itself also plays a stimulatory role in driving chromatin assembly onto RPA coated ssDNA, given that the RPA complex binds H3 to facilitate nucleosome assembly *in vitro* (Liu et al., 2017). In this biochemical study, the chromatin assembly occurred onto naked dsDNA adjacent to the RPA-ssDNA, but the assays included insufficiently long ssDNA to form a nucleosome on ssDNA. By our model, the histone chaperones indirectly facilitate HR by depositing newly-synthesized histones on ssDNA, recruiting a Rad51 loader (Fig. 7F). ASF1 has been implicated in DNA double-strand break repair previously. For example, the budding yeast checkpoint kinase Rad53 (counterpart of human Chk1) binds to ASF1 to regulate its chromatin assembly function (Emili et al., 2001; Hu et al., 2001). More recently, human ASF1A was shown to promote ATM-dependent phosphorylation of MDC1, to facilitate NHEJ (Lee et al., 2017). As such, ASF1 functions in the DNA damage response through various mechanisms.

It is likely that any histones that are assembled by CAF-1 and ASF1 onto ssDNA during HR in human cells are removed upon Rad51 binding. This is suggested by the fact that the ATP-dependent nucleosome remodeler p400 and Rad51 are both required for histone removal from around an induced AsiSI site in human cells (Courilleau et al., 2012). While RPA loading and DNA resection occur normally in the absence of p400, Rad51 is not recruited and histones are not removed from around the DSB (Courilleau et al., 2012). These data suggest that p400 disrupts the nucleosomes from ssDNA to enable Rad51 loading onto the ssDNA. The fact that Rad51 is required for histone removal supports our model that the histones assembled onto ssDNA are displaced upon Rad51 loading (Fig. 7F). The ATP-dependent nucleosome remodeler BRG1 also promotes removal of RPA and replacement with Rad51 (Qi et al., 2015), suggesting that BRG1 may function with ASF1/CAF-1 to either promote chromatin assembly onto ssDNA to displace RPA or to promote chromatin disassembly during Rad51 loading.

Author Manuscript Author Manuscript Author Manuscript Author Manuscript

DNA-PKcs dependent phosphorylation of ASF1A

The chromatin assembly during HR appears to be promoted by DSB-induced phosphorylation of ASF1A on S192 (Fig. 6). This modification promotes the recruitment of ASF1A to chromatin, and increases ASF1A interaction with CAF-1, H3.1 and MMS22L-TONSL (Fig. 6). The involvement of DNA-PKcs in ASF1A phosphorylation provides an elegant mechanism to ensure that the chromatin assembly pathway gets locally stimulated in response to DSBs, given that DNA-PKcs is activated by DNA ends. Indeed, DNA-PKcs is recruited to all DSBs, regardless of whether the DNA breaks are repaired by HR or NHEJ (Caron et al., 2015).

Although DNA-PKcs is not an essential HR protein, it is conceivable that DNA-PKcs-dependent phosphorylation of ASF1A promotes HR. Precedent for non-essential proteins playing a role in HR is provided by ATM. ATM functions in an early step of HR, stimulating end resection through phosphorylation and activation of the nucleases CtIP, MRE11, EXO1 and BLM (Ababou et al., 2000; Lim et al., 2000; Wang et al., 2013; Wu et al., 2000), but ATM is clearly not essential for HR because ATM deficient cells are viable. Interestingly, combined deficiency of ATM and DNA-PKcs leads to early embryonic lethality in mice (Sekiguchi et al., 2001). This fact indicates that DNA-PKcs is doing something important and is potentially consistent with a redundant role of ATM and DNA-PKcs. Indeed, in the setting of NHEJ, DNA-PKcs and ATM function redundantly (Gapud and Sleckman, 2011; Zha et al., 2011), clearly having some overlapping activities. As such, it is conceivable that DNA-PKcs and ATM play partially redundant roles, independent from ASF1A phosphorylation, in HR.

Taken together, we propose a model where chromatin is disassembled around a DSB to enable end resection and RPA loading in human cells (Fig. 7F). DNA-PK is activated by DNA ends to phosphorylate ASF1A which promotes the transient assembly of newly-synthesized histones, seemingly onto the ssDNA. Phosphorylated ASF1 helps recruit MMS22L-TONSL in concert with the affinity of TONSL for newly-synthesized histones, which lack H4 K20me. Once recruited onto the ssDNA, TONSL/MMS22L function to load Rad51 onto ssDNA. In this model, displacement of some RPA is promoted by the transient chromatin assembly, while loading of Rad51 likely displaces the remainder of RPA. We propose that Rad51 loading also drives the subsequent displacement of the histones and their associated epigenetic marks that enabled temporary chromatin compaction around the DSB. Rad51-mediated displacement of the histones and associated MMS22L-TONSL would also provide a mechanism to halt the loading of excessive Rad51 by MMS22L-TONSL. After strand invasion and DNA synthesis have occurred, histones are reassembled onto the dsDNA to complete HR and reset the epigenome.

In summary, genomic processes, such as DSB repair, are facilitated by the local removal of histones from the DNA, to provide access to the DNA lesion. However, an unanticipated aspect of the maintenance of genomic stability suggested by this study is dynamic chromatin reassembly in the midst of homologous recombination onto ssDNA, to promote the specific recruitment of Rad51 to ssDNA. As such, chromatin assembly factors play an active and dynamic role driving the intrinsic steps of DNA repair in human cells, and histones exist on ssDNA during homologous recombination in yeast.

Author Manuscript Author Manuscript Author Manuscript Author Manuscript

STAR Methods

CONTACT FOR REAGENT AND RESOURCE SHARING

Further information and requests for resources and reagents should be directed to and will be fulfilled by the Lead Contact, Jessica Tyler (jet2021@med.cornell.edu).

EXPERIMENTAL MODEL AND SUBJECT DETAILS

Cell lines—HeLa (female), human erythroleukemia K562 (female) and human osteosarcoma U-2 OS (female) cells were grown in complete DMEM, RPMI (Roswell Park Memorial Institute) 1640 Medium and McCoy's 5a Medium, respectively. Human glioma cells M059K and M059J (both male) were maintained in complete DMEM/Ham's F12 Medium. All the above cells were grown at 37°C with 5% CO_2.

METHOD DETAILS

Transfections and DNA damaging agent treatments—For transient transfection, 2×10^6 cells were seeded per 60mm dish for 24 hours prior to the delivery of plasmid DNA using Lipofectamine 2000 (Invitrogen). shRNA viral particles freshly produced from 293T cells were added to desired cells for 2 days to efficiently knockdown gene expressions. To induce DNA damage, cells were generally treated with 40 μg/ml Bleomycin (#9041-93-4, Cayman Chemical Company) and 0.5 μg/ml Neocarzinostatin (#N9162, Sigma-Aldrich) or 5, 10 μM Camptothecin (#C9911, Sigma-Aldrich) or 1000J/M2 UV for 2 hours followed by harvesting at indicated time points after washing with PBS. For experiments where only one time point was analysed, the analysis was performed 24 hrs after Bleomycin removal. ATM inhibitor KU-55933 (#S1092), ATR inhibitor VE-821 (#S8007) and DNA-PK inhibitor NU7026 (#S2893) were purchased from Selleckchem.com. Working concentrations of each inhibitor is indicated in figures/legends. 10 μM of DNA replication inhibitor aphidicolin (APH, #A0781, Sigma-Aldrich) was added to cells for 1 hour prior to combination with Bleomycin for an additional 2 hours. After the removal of drugs, cells were constitutively incubated in APH-contained medium for 24-hour recovery.

siRNA and shRNA knockdowns—Sequences for small RNAis against ASF1A and ASF1B were described in a previous study (Groth et al., 2005) and purchased from Dharmacon. 100 nM of siASF1A and siASF1B were mixed with INTERFERin siRNA transfection reagent (#409-10, Polyplus transfection) according to the manufacturer's protocol to perform ASF1A/B knockdowns for 48 hours. The siRNA control was a random scrambled RNA sequence. Other siRNAs were done using the same method, and the sequences given in Table S2. shRNA lentiviral plasmids against ASF1A, ASF1B, HIRA, CAF-1, DNA-PKcs, Rad51 and the control were obtained from the shRNA and ORFeome Core Facility at the University of Texas MD Anderson Cancer Center (Houston, TX). MMS22L, CtIP and 53BP1 shRNA plasmids were provided through Memorial Sloan Kettering Cancer Center (MSKCC) RNAi core (New York, NY). 293T cells were transfected with shRNA plasmids and the viral packaging vectors pCMV-VSVG and pCMV-dR8.2. The culture media containing shRNA virus particles were collected 48 to 72 hours after transfection and stored at −80 °C. To generate shRNA knockdown cells, cells were incubated with shRNA lentiviral supernatant for 24 hours followed by 1 μg/ml Puromycin

Author Manuscript Author Manuscript Author Manuscript Author Manuscript

for 48 hours. The knockdown efficiency of each target protein was determined by western blotting. Each experiment was repeated at least 3 times and representative results are shown. All siRNA and shRNA target sequences used in this study were list in Table S1.

Alkaline comet assay—2×10^5 K562 cells were pelleted and washed in 1 × PBS followed by resuspension in 1ml 1 × PBS buffer. 1×10^4 cells were added to 45 °C pre-warmed low melting-p oint agarose (#16520050, Invitrogen) to make a final 0.5 % agarose mixture and 50 μl was applied to comet slides (#4250-200-03, Trevigen). The slides were immersed in lysis solution (#4250-010-01, Trevigen) for 1 hour at 4 °C. The slides were immer sed in prechilled unwinding buffer (0.3N NaOH and 1mM EDTA, pH13.1) for another 30 minutes at 4 °C followed by electrophoresis at 1.5 V cm^{-1} for 15 minutes at room temperature. After electrophoresis, nuclear DNA was counterstained with CyberGold.

HR repair assay—HR repair analysis was performed as described previously (Nakanishi et al., 2011) using DR-GFP-U2-OS cells. 5×10^6 shscrambled and 2-day post viral transduction cells were plated onto 100 mm dishes O/N. 18 μg I-SceI plasmid was transfected with Lipofectamine 2000 for 6 hours followed by replacement with fresh McCoy's 5A medium and 48-hour incubation. All samples were collected and directly analysed by Flow cytometry.

Flow cytometry analysis—To analyse DNA content of cells, harvested cells were washed in PBS with 1% FBS followed by fixation in 70% ethanol overnight at 4 °C. Fixed cells were spun down to aspirate ethanol and then were washed in PBS once. Cell pellets were resuspended in PBS with 1% FBS containing 10 μg/ml propidium iodide (PI) (#81845, Sigma-Aldrich) and 0.5 μg/ml RNase A (#10109142001, Sigma-Aldrich) and kept in the dark at room temperature for 1 hour. For HR repair assay, harvested cells were resuspended in PBS with 1% FBS and were directly subjected to flow cytometry analysis using BD LSRII flow cytometer.

Immunofluorescence analysis—Cells were plated on poly-L-lysine-coated coverslips for 24 hours. After bleomycin treatment, coverslips were washed with PBS. For DNA damage foci analysis, 0.1 % Triton-X-100 in cytoskeletal (CSK) buffer (100 mM NaCl, 300 mM sucrose, 3 mM $MgCl_2$, 10 mM PIPES (pH 6.8)) was added to permeabilize cells for 3 minutes at room temperature. Cells were washed once with TBS-T (0.05 % Tween-20) and fixed with 4 % paraformaldehyde for 10 minutes. Fixed cells were blocked with 3 % BSA for 30 minutes. Primary antibodies diluted in 3 % BSA blocking buffer were subsequently incubated with coverslips overnight at 4 °C. Cells were washed 3 times with TBS-T before incubating with fluorescence conjugated-secondary antibodies for 1 hour at room temperature in the dark. After washing in PBS, cells were mounted in prolong gold antifade mountant with DAPI and kept at 4 °C in the dark. Cells were imaged using a 3i confocal microscope system or Olympus BX53 camera and were analysed via ImageJ software.

Protein extraction and immunoblotting—After washing once in PBS, cells were resuspended in pre-chilled RIPA buffer (50 mM Tris-HCl, pH7.4, 1 mM EDTA, 0.5 mM EGTA, 1 % Triton-X-100, 0.1 % Nadeoxycholate, 0.1 % SDS, 150 mM NaCl, protease inhibitors (complete Mini EDTA-free, #4693159001, Roche) and phosphatase inhibitors

Author Manuscript Author Manuscript Author Manuscript Author Manuscript

(PhosSTOP, #4906837001, Roche) followed by sonication. Cell debris was removed by centrifugation at 14,000 *r.p.m.*, at 4 °C for 10 minutes. Supernatants were collect ed and protein concentrations quantitated by Bradford protein assay (#500-0006, Bio-Rad). Equivalent protein amounts were loaded on SDS-PAGE or Criterion 4-12 % precast gels (#5671085, Bio-Rad). After electrophoresis, proteins were transferred to Nitrocellulose membrane (#10600048, GE Healthcare Life Sciences) for 90 minutes at 4 °C and membranes were incubated with 5 % non-f at milk for 1 hour at room temperature before overnight incubation with diluted primary antibodies at 4 °C, followed by incubation with secondary antibodies in 5 % non-fat milk for 1 hour at room temperature. To detect ASF1 phosphorylation after DNA damage, cells had to be scraped off the plates, not trypsinized. Enhanced chemiluminescence (ECL) Western blotting substrate (# RPN 3243, Amersham ECL, GE Healthcare Life Sciences) were used for detection, using a protein simple analysis machine.

Ectopic expression of wild type and mutant ASF1A—HA tagged wild type (HA-WT) and mutant human ASF1A (HA-S192A) (a generous gift from Dr. Yuri M. Moshkin) were expressed from pcDNA3.1 (+) vector. Other mutations were generated with the HA-WT plasmid as a template by site directed mutagenesis to make the V94R and S192D substitutions. All the above plasmids had been made immune to knockdown of endogenous ASF1A by nucleotide mutation of seed sequence "AGATGC" to "CGAGGC" (Table S1).

Immunoprecipitation—2×10^6 HeLa cells were seeded into 60mm dishes and incubated overnight. HA-tagged ASF1A plasmids (HA-WT, HA-V94R, HA-S192A and HA-S192D) were transfected into cells for 24 hours before harvesting. Cells were then lysed with pre-chilled modified RIPA buffer (replace 1 % Triton X-100 with 0.5 % NP-40) for 15 minutes on ice. To collect supernatant, lysates were centrifuged at 14,000 *r.p.m.* at 4 °C for 10 minutes. Cell lysates were precleared with Dynabeads Protein A (#10001D, ThermoFisher Scientific) for 1 hour followed by incubation with anti-HA-Agarose (#A2095, clone HA-7, Sigma-Aldrich) for 3 hours at 4 °C. After centrifugation, the HA-Agarose protein complexes were washed in RIPA buffer 3 times for 15 minutes and boiled with SDS loading buffer.

Chromatin fractionation analysis—This analysis was performed as described previously with slight modification (Méndez and Stillman, 2000). Whole cell extract (WCE) samples were taken from the same batch of samples used for chromatin fractionation and prepared separately. Cells harvested from 6-well plates were re-suspended in buffer A (10 mM HEPES, pH7.9, 10 mM KCl, 1.5 mM $MgCl_2$, 0.34 M sucrose, 10 % glycerol, 1 mM DTT, complete Mini (EDTA-free) protease and PhosSTOP phosphatase inhibitors) before adding an equal volume of buffer A with 0.2 % Triton X-100 and were incubated on ice for 4.5 minutes. Cytoplasmic protein fractions were collected after centrifuge at 1,300 × g, for 4 minutes at 4 °C. The insoluble pellet, including chromatin, was washed with buffer A and then the supernatant was aspirated. The pellet was resuspended in buffer B (3 mM EDTA, 0.2 mM EGTA, 1 mM DTT, complete Mini protease and PhosSTOP phosphatase inhibitors) for 15 minutes, followed by centrifugation at 1,700 × g, 4 minutes at 4 °C. Nuc lear protein fractions were obtained from the supernatant. Wash pellet once in buffer B and apply S7

Author Manuscript Author Manuscript Author Manuscript Author Manuscript

nuclease and RIPA buffer with 5 mM $CaCl_2$ to each sample for 10 minutes on ice, followed by sonication to solubilize. This is referred to as the “chromatin” fraction.

Native BrdU resection assay—Cells were seeded in 24-well plates containing coverslips overnight and were incubated with 30 μM BrdU (#550891, BD Biosciences) for an additional 48 hours followed by the treatment of DNA damaging agents (Bleomycin or CPT) for the time periods indicated in the figures. CtIP and 53BP1-depleted cells serve as negative and positive controls, respectively, for DNA end resection. After treatment, the same steps were carried out that were described in the immunofluorescence analysis except that the diluted anti-BrdU antibody (1:400, #555627, BD Biosciences) was applied to samples at room temperature for 2 hours. Cells were imaged using an Olympus BX53 microscope system and images were captured via Cell Sense and photoshop software. For measuring BrdU intensity, 100 cells of each sample were quantitated by Fiji (ImageJ) software.

AsiSI DNA resection assay—The amount of ssDNA generated after a DSB was measured as previously described (Iacovoni et al., 2010). Briefly ER-AsiSI 293T cells (gift from Dr. Tanya Paull) were transfected with siRNA using Interferin (#409-50, Polyplus Transfection) for 48-72 hours. Then, cells were treated or not for 4 hours with 300 nM 4OHT (T5648, Sigma-Aldrich) to induce ER-AsiSI localization into the nucleus. DNA was purified using the QIAGEN QIAamp DNA Mini kit. 140 ng of genomic DNA was then digested or not with 20 units of restriction enzymes (BsrgI or HindIII). 5.6 ng of digested or undigested genomic DNA was then used as a template in a 10 μl qPCR reaction with 5 μl of SYBR Green I Master Mix (#04707516001, Roche) on a Roche Lightcycler 480 II qPCR machine. Primers used in the reaction were published previously (Zhou et al., 2014). To calculate %ssDNA, a ΔCt value was calculated by subtracting the Ct value of the undigested sample from the Ct value of the digested sample. This ΔCt value was then normalized to the ΔCt value of a random site in the genome (HindIII digestion site). The %ssDNA was calculated using the equation ssDNA% = 1/(2^(ΔCt−1) + 0.5)*100.

ChIP analysis of H3—ChIP analysis was performed as previously described (Chen et al., 2008). In brief, Yeast cells (Strain JKM179 from Jim Haber MATα ade1 leu2-3,112 lys5 trp1::hisG ura3-52) were cultured in YEP medium containing lactic acid. HO endonuclease was induced by addition of 2% galactose to generate a DSB. At indicated time points, 5×10^7 yeast cells were harvested and protein-DNA complexes were cross-linked with formaldehyde. After shearing of the chromatin, an antibody to the C-terminus of H3 (#1791, Abcam) was used for immunoprecipitation. Quantitation of the DNA molecules present in immunoprecipitates was performed by qPCR using a Roche 480 instrument with the primers listed in Table S2, normalizing to a gene product from SMC2 in each sample.

QUANTIFICATION AND STATISTICAL ANALYSIS

For the comet assay, 100 cells of each sample (n=2) from × 100 magnifications images were scored to calculate tail moment (a.u.) using ImageJ software. For all histograms of foci analysis, 100 cells of each sample were quantitated by Fiji (ImageJ) software. The statistical

Author Manuscript Author Manuscript Author Manuscript Author Manuscript

tests, number of individual experimental repeats, the dispersion and precision measures (median, SD or SEM) are indicated in the figure legends.

DATA AND SOFTWARE AVAILIBILITY

Raw images that were analysed for this manuscript are available as a Mendeley dataset http://dx.doi.org/10.17632/7rzzn46jvy.1

KEY RESOURCES TABLE

REAGENT or RESOURCE	SOURCE	IDENTIFIER
Antibodies		
ASF1A	Cell Signaling Technology	Cat# 2990S; RRID: AB_2289918
ASF1B	Thermo Fisher Scientific	Cat# MA5-14836; RRID: AB_10977557
ATM	Cell Signaling Technology	Cat# 2873S; RRID: AB_2062659
ATR (H-300)	Santa Cruz Biotechnology	Cat# sc-1887; RRID: AB_630893
BrdU (bromodeoxyuridine)	BD Biosciences	Cat# 555627; RRID: AB_10015222
CAF-1 p150	Santa Cruz Biotechnology	Cat# sc-133105; RRID: AB_2079444
CAF-1 p60	BETHYL	Cat# A301-085A; RRID: AB_872991
Cdc2	GeneTex	Cat# GTX108120; RRID: AB_1949938
Chk1	Santa Cruz Biotechnology	Cat# sc-8408; RRID: AB_627257
DNA-PKcs	Cell Signaling Technology	Cat# 4602S; RRID: AB_10692482
GAPDH	Abcam	Cat# ab8245; RRID: AB_2107448
HA	Covance Research Products Inc	Cat# MMS-101R; RRID: AB_291263
HIRA	Active Motif	Cat# 39557
Histone H3	Abcam	Cat# ab1791; RRID: AB_302613
Histone H4	Active Motif	Cat# 39269; RRID: AB_2636967
MMS22L	Àbcam	Cat# ab181047
Orc2	BD Biosciences	Cat# 51-6875GR
Rad51	Abcam	Cat# ab213; RRID: AB_302856
RPA34	Millipore	Cat# NA19L; RRID: AB_565123
TLK1	Thermo Fisher Scientific	Cat# PA5-17576; RRID: AB_10983566
TLK2	GeneTex	Cat# GTX32923
TONSL	Abcam	Cat# ab101898; RRID: AB_10898931
α-tubulin	Sigma-Aldrich	Cat# T9026; RRID: AB_477593
Vinculin	Cell Signaling Technology	Cat# 4650; RRID: AB_10559207
Phospho-ATM (S1981)	Abcam	Cat# 79891; RRID: AB_10670395
Phospho-cdc2 (Tyr15)	Cell Signaling Technology	Cat# 9111S; RRID: AB_10835695
Phospho-Chk1 (S345)	Cell Signaling Technology	Cat# 2341S; RRID: AB_330023
Phospho-RAD9 (S328)	Abgent	Cat# AP3225a; RRID: AB_637777
Phospho-RPA32 (S4/S8)	BETHYL	Cat# A300-245A; RRID: AB_210547
Chemicals, Peptides, and Recombinant Proteins		
Bleomycin (Bleo)	Cayman Chemical Company	Cat# 9041-93-4

Author Manuscript Author Manuscript Author Manuscript Author Manuscript

REAGENT or RESOURCE	SOURCE	IDENTIFIER
Neocarzinostatin (NCS)	Sigma-Aldrich	Cat# N9162
Camptothecin (CPT)	Sigma-Aldrich	Cat# C9911
BrdU	BD Biosciences	Cat# 550891
Lepofectamine 2000 Transfection Reagent	Thermo Fisher Scientific	Cat# 11668500
INTERFERin siRNA Transfection Reagent	Polyplus transfection	Cat# 409-10
ATM inhibitor KU-55933	Selleckchem.com	Cat# S1092
ATR inhibitor VE-821	Selleckchem.com	Cat# S8007
DNA-PK inhibitor NU7026	Selleckchem.com	Cat# S2893
DNA replication inhibitor Aphidicolin (APH)	Sigma-Aldrich	Cat# A0781
Protease inhibitors Complete Mini EDTA-free	Roche	Cat# 4693159001
Phosphatase inhibitors PhosSTOP	Roche	Cat# 4906837001
Low melting-point agarose	Thermo Fisher Scientific	Cat# 16520050
Propidium iodide (PI)	Sigma-Aldrich	Cat# 81845
RNase A	Sigma-Aldrich	Cat# 10109142001
4-OHT	Sigma-Aldrich	Cat# T5648
Nuclease S7	Sigma-Aldrich	Cat# 10107921001
Critical Commercial Assays		
Comet Slide	Trevigen	Cat# 4250-200-03
Lysis solution	Trevigen	Cat# 4250-010-01
Dynabeads Protein A	Thermo Fisher Scientific	Cat# 10001D
Anti-HA Agarose (Clone HA-7)	Sigma-Aldrich	Cat# A2095
Bradford protein assay	Bio-Rad	Cat# 500-0006
Enhanced chemiluminescence Western blotting substrate (ECL)	GE Healthcare Life Sciences	Cat# RPN 3243
SYBR Green I Master Mix	Roche	Cat# 04707516001
Experimental Models: Cell Lines		
HeLa cells	ATCC	Cat# CCL-2; RRID: CVCL_0030
K-562 cells	ATCC	Cat# CCL-243; RRID: CVCL_0004
U-2 OS cells	ATCC	Cat# HTB-96; RRID: CVCL_0042
M059J	ATCC	Cat# CRL-2366; RRID: CVCL_0400
M059K	ATCC	Cat# CRL-2365; RRID: CVCL_0401
DR-GFP-U-2 OS cells	Laboratory of Maria Jasin	N/A
ER-AsiSI 293T cells	Zhou et al., 2014	https://doi.org/10.1093/nar/gkt 1309
Experimental Models: Organisms/Strains		
Yeast cells JKM179	Laboratory of Jim Haber	MATα ade1 leu2-3,112 lys5 trp1::hisG ura3-52
Oligonucleotides		
shRNA targeting sequences, see Table S1	Dharmacon/Sigma-Aldrich	N/A

Author Manuscript Author Manuscript Author Manuscript Author Manuscript

REAGENT or RESOURCE	SOURCE	IDENTIFIER
siRNA targeting sequences, see Table S1	Dharmacon	N/A
Primers for ChIP analysis See Table S2	This paper	N/A
Recombinant DNA		
I-SceI plasmid	Laboratory of Hui-Kuan Lin	N/A
HA-WT	Laboratory of Yuri M. Moshkin	N/A
HA-S192A	Laboratory of Yuri M. Moshkin	N/A
HA-V94R	This paper	N/A
HA-S192D	This paper	N/A
Software and Algorithms		
ImageJ	NIH	https://imagej.nih.gov/ij/
FlowJo	FlowJo	https://www.flowjo.com
Deposited Data		
Mendeley dataset http://dx.doi.org/10.17632/7rz zn46jvy.1		

Supplementary Material

Refer to Web version on PubMed Central for supplementary material.

Acknowledgments

We are grateful to Yuri Moshkin for HA tagged ASF1A plasmids and Maria Jasin for the U-2 OS DR-GFP cell line and Hui-Kuan Lin for the I-SceI plasmid. Thanks to Gaelle Legube and Tanya Paull for reagents for the AsiSI resection assay and to Jim Haber for yeast strains. We thank the shRNA and ORFeome Core Facility at the University of Texas MD Anderson Cancer Center and Memorial Sloan Kettering Cancer Center (MSKCC) RNAi core for providing shRNA clones. We are highly grateful to Bo-Ruei Chen for helpful suggestions on the manuscript. This work was supported by grant NCI CA95641 to JKT.

References

Ababou M, Dutertre S, Lecluse Y, Onclercq R, Chatton B, Amor-Gueret M. ATM-dependent phosphorylation and accumulation of endogenous BLM protein in response to ionizing radiation. Oncogene. 2000; 19:5955–5963. [PubMed: 11146546]

Adam S, Polo SE, Almouzni G. Transcription recovery after DNA damage requires chromatin priming by the H3.3 histone chaperone HIRA. Cell. 2013; 155:94–106. [PubMed: 24074863]

Adkins NL, Swygert SG, Kaur P, Niu H, Grigoryev SA, Sung P, Wang H, Peterson CL. Nucleosome-like, ssDNA-histone octamer complexes and the implication for DNA double-strand break repair. J Biol Chem. 2017

Baldeyron C, Soria G, Roche D, Cook AJL, Almouzni G. HP1alpha recruitment to DNA damage by p150CAF-1 promotes homologous recombination repair. J Cell Biol. 2011; 193:81–95. [PubMed: 21464229]

Bekker-Jensen S, Lukas C, Kitagawa R, Melander F, Kastan MB, Bartek J, Lukas J. Spatial organization of the mammalian genome surveillance machinery in response to DNA strand breaks. J Cell Biol. 2006; 173:195–206. [PubMed: 16618811]

Berkovich E, Monnat RJ Jr, Kastan MB. Roles of ATM and NBS1 in chromatin structure modulation and DNA double-strand break repair. Nat Cell Biol. 2007; 9:683–690. [PubMed: 17486112]

Author Manuscript Author Manuscript Author Manuscript Author Manuscript

Caron P, Choudjaye J, Clouaire T, Bugler B, Daburon V, Aguirrebengoa M, Mangeat T, Iacovoni JS, Alvarez-Quilon A, Cortes-Ledesma F, et al. Non-redundant Functions of ATM and DNA-PKcs in Response to DNA Double-Strand Breaks. Cell reports. 2015; 13:1598–1609. [PubMed: 26586426]

Chapman JR, Taylor MR, Boulton SJ. Playing the end game: DNA double-strand break repair pathway choice. Molecular cell. 2012; 47:497–510. [PubMed: 22920291]

Chen CC, Carson JJ, Feser J, Tamburini B, Zabaronick S, Linger J, Tyler JK. Acetylated lysine 56 on histone H3 drives chromatin assembly after repair and signals for the completion of repair. Cell. 2008; 134:231–243. [PubMed: 18662539]

Ciccia A, Elledge SJ. The DNA damage response: making it safe to play with knives. Molecular cell. 2010; 40:179–204. [PubMed: 20965415]

Courilleau C, Chailleux C, Jauneau A, Grimal F, Briois S, Boutet-Robinet E, Boudsocq F, Trouche D, Canitrot Y. The chromatin remodeler p400 ATPase facilitates Rad51-mediated repair of DNA double-strand breaks. J Cell Biol. 2012; 199:1067–1081. [PubMed: 23266955]

Diao LT, Chen CC, Dennehey B, Pal S, Wang P, Shen ZJ, Deem A, Tyler JK. Delineation of the role of chromatin assembly and the Rtt101Mms1 E3 ubiquitin ligase in DNA damage checkpoint recovery in budding yeast. PloS one. 2017; 12:e0180556. [PubMed: 28749957]

Duro E, Lundin C, Ask K, Sanchez-Pulido L, MacArtney TJ, Toth R, Ponting CP, Groth A, Helleday T, Rouse J. Identification of the MMS22L-TONSL complex that promotes homologous recombination. Mol Cell. 2010; 40:632–644. [PubMed: 21055984]

Emili A, Schieltz DM, Yates JR 3rd, Hartwell LH. Dynamic interaction of DNA damage checkpoint protein Rad53 with chromatin assembly factor Asf1. Mol Cell. 2001; 7:13–20. [PubMed: 11172707]

Gapud EJ, Sleckman BP. Unique and redundant functions of ATM and DNA-PKcs during V(D)J recombination. Cell Cycle. 2011; 10:1928–1935. [PubMed: 21673501]

Goldstein M, Derheimer FA, Tait-Mulder J, Kastan MB. Nucleolin mediates nucleosome disruption critical for DNA double-strand break repair. Proc Natl Acad Sci U S A. 2013; 110:16874–16879. [PubMed: 24082117]

Groth A, Corpet A, Cook AJ, Roche D, Bartek J, Lukas J, Almouzni G. Regulation of replication fork progression through histone supply and demand. Science. 2007; 318:1928–1931. [PubMed: 18096807]

Groth A, Lukas J, Nigg EA, Sillje HH, Wernstedt C, Bartek J, Hansen K. Human Tousled like kinases are targeted by an ATM- and Chk1-dependent DNA damage checkpoint. EMBO J. 2003; 22:1676–1687. [PubMed: 12660173]

Groth A, Ray-Gallet D, Quivy JP, Lukas J, Bartek J, Almouzni G. Human Asf1 regulates the flow of S phase histones during replicational stress. Mol Cell. 2005; 17:301–311. [PubMed: 15664198]

Hammond CM, Stromme CB, Huang H, Patel DJ, Groth A. Histone chaperone networks shaping chromatin function. Nature reviews. Molecular cell biology. 2017; 18:141–158. [PubMed: 28053344]

Hoek M, Stillman B. Chromatin assembly factor 1 is essential and couples chromatin assembly to DNA replication in vivo. Proc Natl Acad Sci U S A. 2003; 100:12183–12188. [PubMed: 14519857]

Hu F, Alcasabas AA, Elledge SJ. Asf1 links Rad53 to control of chromatin assembly. Genes Dev. 2001; 15:1061–1066. [PubMed: 11331602]

Iacovoni JS, Caron P, Lassadi I, Nicolas E, Massip L, Trouche D, Legube G. High-resolution profiling of gammaH2AX around DNA double strand breaks in the mammalian genome. EMBO J. 2010; 29:1446–1457. [PubMed: 20360682]

Jackson SP, Bartek J. The DNA-damage response in human biology and disease. Nature. 2009; 461:1071–1078. [PubMed: 19847258]

Kim JA, Haber JE. Chromatin assembly factors Asf1 and CAF-1 have overlapping roles in deactivating the DNA damage checkpoint when DNA repair is complete. Proc Natl Acad Sci U S A. 2009; 106:1151–1156. [PubMed: 19164567]

Klimovskaia IM, Young C, Strømme CB, Menard P, Jasencakova Z, Mejlvang J, Ask K, Ploug M, Nielsen ML, Jensen ON, et al. Tousled-like kinases phosphorylate Asf1 to promote histone supply during DNA replication. Nat Commun. 2014; 5:3394. [PubMed: 24598821]

Author Manuscript Author Manuscript Author Manuscript Author Manuscript

Kornberg RD. Chromatin structure: a repeating unit of histones and DNA. Science. 1974; 184:868–871. [PubMed: 4825889]

Lee KY, Im JS, Shibata E, Dutta A. ASF1a Promotes Non-homologous End Joining Repair by Facilitating Phosphorylation of MDC1 by ATM at Double-Strand Breaks. Mol Cell. 2017; 68:61–75 e65. [PubMed: 28943310]

Lewis LK, Karthikeyan G, Cassiano J, Resnick MA. Reduction of nucleosome assembly during new DNA synthesis impairs both major pathways of double-strand break repair. Nucleic Acids Res. 2005; 33:4928–4939. [PubMed: 16141196]

Li X, Tyler JK. Nucleosome disassembly during human non-homologous end joining followed by concerted HIRA- and CAF-1-dependent reassembly. eLife. 2016; 5

Lim DS, Kim ST, Xu B, Maser RS, Lin J, Petrini JH, Kastan MB. ATM phosphorylates p95/nbs1 in an S-phase checkpoint pathway. Nature. 2000; 404:613–617. [PubMed: 10766245]

Lin YF, Shih HY, Shang Z, Matsunaga S, Chen BP. DNA-PKcs is required to maintain stability of Chk1 and Claspin for optimal replication stress response. Nucleic Acids Res. 2014; 42:4463–4473. [PubMed: 24500207]

Liu S, Opiyo SO, Manthey K, Glanzer JG, Ashley AK, Amerin C, Troksa K, Shrivastav M, Nickoloff JA, Oakley GG. Distinct roles for DNA-PK, ATM and ATR in RPA phosphorylation and checkpoint activation in response to replication stress. Nucleic Acids Res. 2012; 40:10780–10794. [PubMed: 22977173]

Liu S, Xu Z, Leng H, Zheng P, Yang J, Chen K, Feng J, Li Q. RPA binds histone H3-H4 and functions in DNA replication-coupled nucleosome assembly. Science. 2017; 355:415–420. [PubMed: 28126821]

Loyola A, Bonaldi T, Roche D, Imhof A, Almouzni G. PTMs on H3 variants before chromatin assembly potentiate their final epigenetic state. Mol Cell. 2006; 24:309–316. [PubMed: 17052464]

Marechal A, Zou L. DNA damage sensing by the ATM and ATR kinases. Cold Spring Harbor perspectives in biology. 2013; 5

Mehta A, Haber JE. Sources of DNA double-strand breaks and models of recombinational DNA repair. Cold Spring Harbor perspectives in biology. 2014; 6:a016428. [PubMed: 25104768]

Mello JA, Sillje HH, Roche DM, Kirschner DB, Nigg EA, Almouzni G. Human Asf1 and CAF-1 interact and synergize in a repair-coupled nucleosome assembly pathway. EMBO Rep. 2002; 3:329–334. [PubMed: 11897662]

Méndez J, Stillman B. Chromatin association of human origin recognition complex, cdc6, and minichromosome maintenance proteins during the cell cycle: assembly of prereplication complexes in late mitosis. Mol Cell Biol. 2000; 20:8602–8612. [PubMed: 11046155]

Mousson F, Lautrette A, Thuret JY, Agez M, Courbeyrette R, Amigues B, Becker E, Neumann JM, Guerois R, Mann C, et al. Structural basis for the interaction of Asf1 with histone H3 and its functional implications. Proc Natl Acad Sci U S A. 2005; 102:5975–5980. [PubMed: 15840725]

Nakanishi K, Cavallo F, Brunet E, Jasin M. Homologous recombination assay for interstrand cross-link repair. Methods Mol Biol. 2011; 745:283–291. [PubMed: 21660700]

O'Donnell L, Panier S, Wildenhain J, Tkach JM, Al-Hakim A, Landry MC, Escribano-Diaz C, Szilard RK, Young JT, Munro M, et al. The MMS22L-TONSL complex mediates recovery from replication stress and homologous recombination. Mol Cell. 2010; 40:619–631. [PubMed: 21055983]

Palter KB, Foe VE, Alberts BM. Evidence for the formation of nucleosome-like histone complexes on single-stranded DNA. Cell. 1979; 18:451–467. [PubMed: 498278]

Pierce AJ, Johnson RD, Thompson LH, Jasin M. XRCC3 promotes homology-directed repair of DNA damage in mammalian cells. Genes Dev. 1999; 13:2633–2638. [PubMed: 10541549]

Piwko W, Olma MH, Held M, Bianco JN, Pedrioli PG, Hofmann K, Pasero P, Gerlich DW, Peter M. RNAi-based screening identifies the Mms22L-Nfkbil2 complex as a novel regulator of DNA replication in human cells. EMBO J. 2010; 29:4210–4222. [PubMed: 21113133]

Polo SE, Almouzni G. Chromatin dynamics after DNA damage: The legacy of the access-repair-restore model. DNA Repair (Amst). 2015; 36:114–121. [PubMed: 26429064]

Author Manuscript Author Manuscript Author Manuscript Author Manuscript

Qi W, Wang R, Chen H, Wang X, Xiao T, Boldogh I, Ba X, Han L, Zeng X. BRG1 promotes the repair of DNA double-strand breaks by facilitating the replacement of RPA with RAD51. Journal of cell science. 2015; 128:317–330. [PubMed: 25395584]

Raderschall E, Golub EI, Haaf T. Nuclear foci of mammalian recombination proteins are located at single-stranded DNA regions formed after DNA damage. Proc Natl Acad Sci U S A. 1999; 96:1921–1926. [PubMed: 10051570]

Saredi G, Huang H, Hammond CM, Alabert C, Bekker-Jensen S, Forne I, Reveron-Gomez N, Foster BM, Mlejnkova L, Bartke T, et al. H4K20me0 marks post-replicative chromatin and recruits the TONSL-MMS22L DNA repair complex. Nature. 2016; 534:714–718. [PubMed: 27338793]

Sarraf SA, Stancheva I. Methyl-CpG binding protein MBD1 couples histone H3 methylation at lysine 9 by SETDB1 to DNA replication and chromatin assembly. Mol Cell. 2004; 15:595–605. [PubMed: 15327775]

Sartori AA, Lukas C, Coates J, Mistrik M, Fu S, Bartek J, Baer R, Lukas J, Jackson SP. Human CtIP promotes DNA end resection. Nature. 2007; 450:509–514. [PubMed: 17965729]

Sekiguchi J, Ferguson DO, Chen HT, Yang EM, Earle J, Frank K, Whitlow S, Gu Y, Xu Y, Nussenzweig A, et al. Genetic interactions between ATM and the nonhomologous end-joining factors in genomic stability and development. Proc Natl Acad Sci U S A. 2001; 98:3243–3248. [PubMed: 11248063]

Shaltiel IA, Krenning L, Bruinsma W, Medema RH. The same, only different - DNA damage checkpoints and their reversal throughout the cell cycle. Journal of cell science. 2015; 128:607–620. [PubMed: 25609713]

Song Y, He F, Xie G, Guo X, Xu Y, Chen Y, Liang X, Stagljar I, Egli D, Ma J, et al. CAF-1 is essential for Drosophila development and involved in the maintenance of epigenetic memory. Dev Biol. 2007; 311:213–222. [PubMed: 17916346]

Sunavala-Dossabhoy G, De Benedetti A. Tousled homolog, TLK1, binds and phosphorylates Rad9; TLK1 acts as a molecular chaperone in DNA repair. DNA Repair (Amst). 2009; 8:87–102. [PubMed: 18940270]

Wang H, Shi LZ, Wong CC, Han X, Hwang PY, Truong LN, Zhu Q, Shao Z, Chen DJ, Berns MW, et al. The interaction of CtIP and Nbs1 connects CDK and ATM to regulate HR-mediated double-strand break repair. PLoS genetics. 2013; 9:e1003277. [PubMed: 23468639]

Williamson EA, Wray JW, Bansal P, Hromas R. Overview for the histone codes for DNA repair. Prog Mol Biol Transl Sci. 2012; 110:207–227. [PubMed: 22749147]

Wu X, Ranganathan V, Weisman DS, Heine WF, Ciccone DN, O'Neill TB, Crick KE, Pierce KA, Lane WS, Rathbun G, et al. ATM phosphorylation of Nijmegen breakage syndrome protein is required in a DNA damage response. Nature. 2000; 405:477–482. [PubMed: 10839545]

Xu Y, Price BD. Chromatin dynamics and the repair of DNA double strand breaks. Cell Cycle. 2011; 10:261–267. [PubMed: 21212734]

Zha S, Jiang W, Fujiwara Y, Patel H, Goff PH, Brush JW, Dubois RL, Alt FW. Ataxia telangiectasia-mutated protein and DNA-dependent protein kinase have complementary V(D)J recombination functions. Proc Natl Acad Sci U S A. 2011; 108:2028–2033. [PubMed: 21245310]

Zhou Y, Caron P, Legube G, Paull TT. Quantitation of DNA double-strand break resection intermediates in human cells. Nucleic Acids Res. 2014; 42:e19. [PubMed: 24362840]

Author Manuscript Author Manuscript Author Manuscript Author Manuscript

Highlights

- ASF1 and CAF-1 promote Rad51 loading during homologous recombination in human cells
- ASF1 and CAF-1 help recruit the Rad51 loader MMS22L/TONSL to DNA breaks
- Knockdown of ASF1 or Rad51 leads to persistent DNA end resection in human cells
- End-resected single-strand DNA is occupied by histones in yeast

Author Manuscript Author Manuscript Author Manuscript Author Manuscript

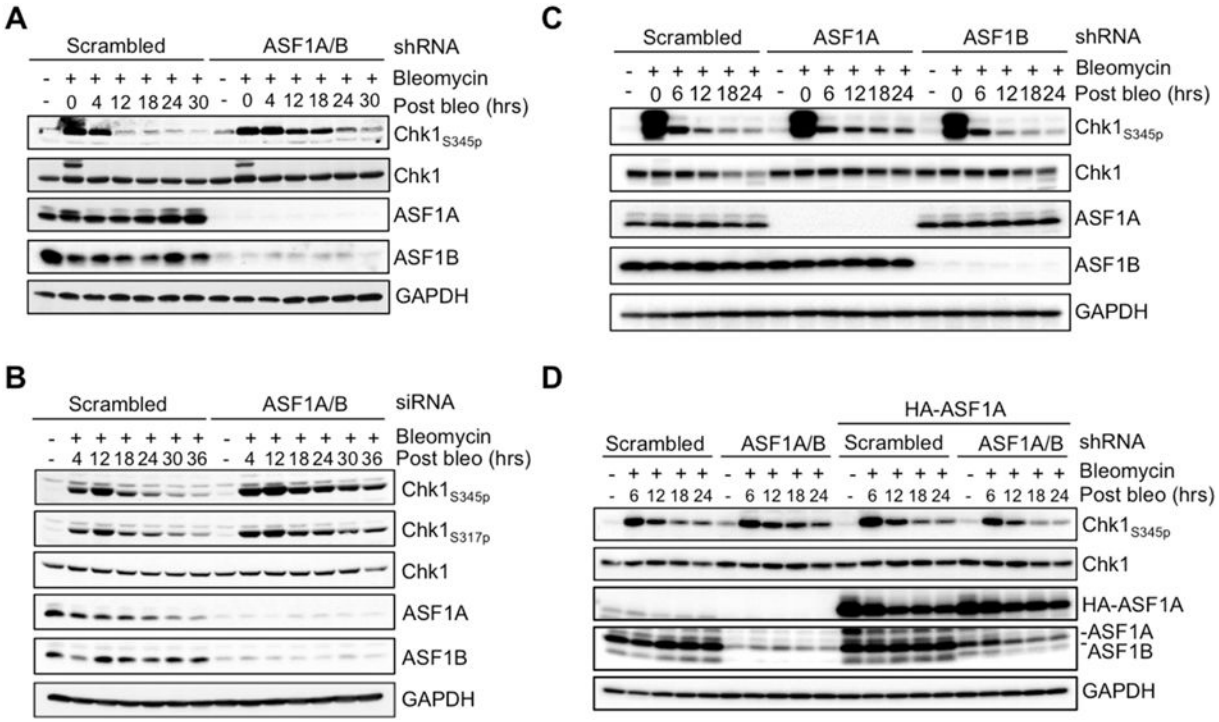

Figure 1. ASF1A is required for timely inactivation of Chk1

(A) HeLa cells transduced with lentiviruses expressing scrambled shRNA or shRNA against both ASF1A and ASF1B for 72 hours were treated with 40 μg/ml bleomycin for 2 hours, following by washing out the bleomycin at time 0. Samples were taken at the indicated time points after washing out the bleomycin. (B) Protein expression of ASF1A/B was silenced by siRNA-mediated knockdown for 48 hours, followed by bleomycin treatment as described in (A). (C) As in A, but with individual knockdown of either ASF1A or ASF1B. (D) Knockdowns were performed as described in (A), followed by transiently transducing with HA-tagged $ASF1A^{WT}$. Then the experiment was performed as described in (A). All results were obtained at least three independent times, and representative results are shown. See also Figure S1.

Author Manuscript Author Manuscript Author Manuscript Author Manuscript

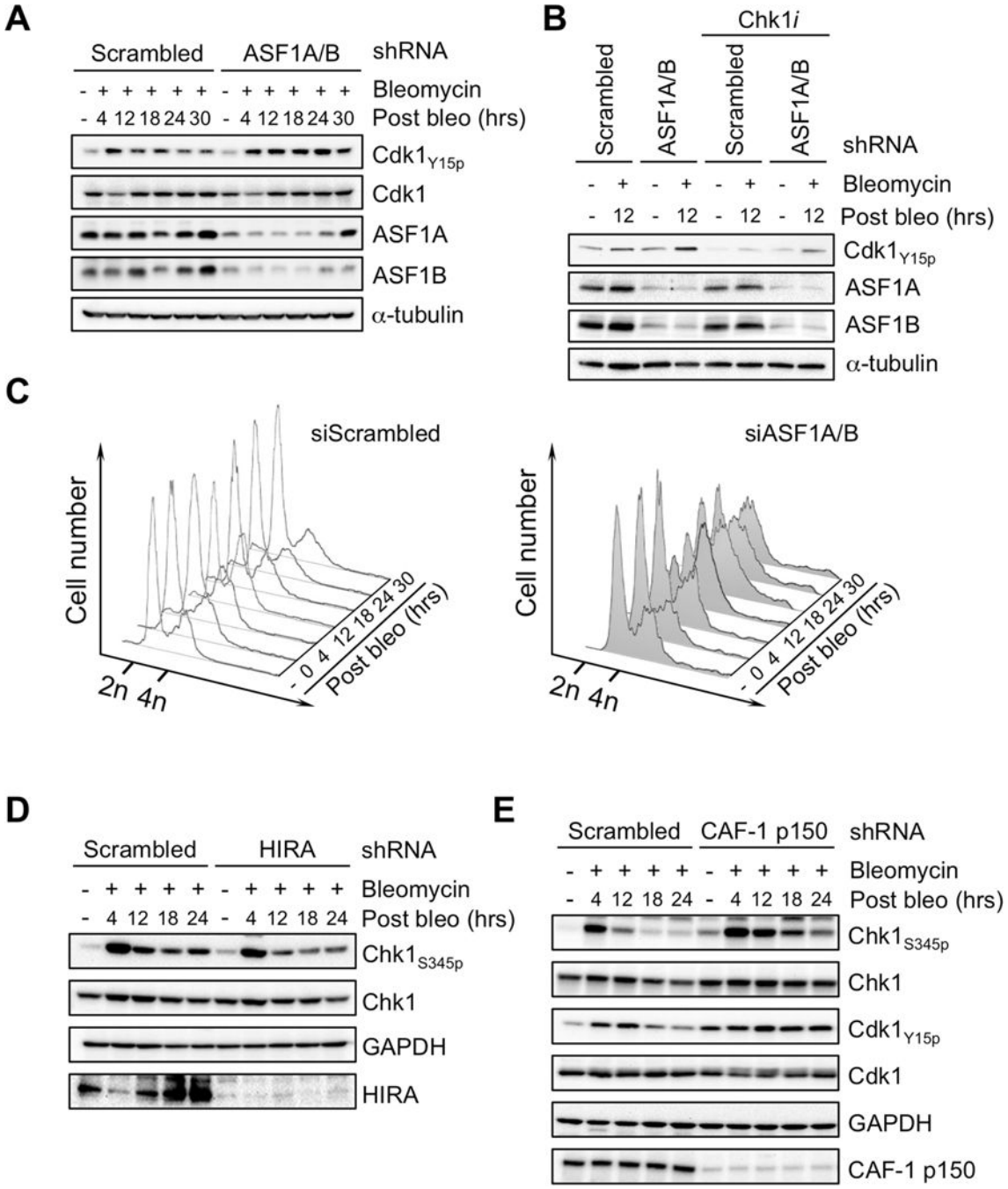

Figure 2. Depletion of CAF-1, but not HIRA, phenocopies the prolonged Chk1 phosphorylation and the delay of cell cycle progression in ASF1 knockdown cells

(A) The experiment was performed as described in Fig. 1A, with western blotting for the indicated proteins or modification. (B) Chk1 plays a major role in promoting $Cdk1_{Y15}$ phosphorylation in ASF1 depleted cells. 10 μM of Chk1 inhibitor, AZD7762, was added to cells for an hour followed by co-incubating with bleomycin for an additional 2 hours. After bleomycin removal, 10 μM of Chk1 inhibitor was re-applied for 12 hours. (C) Propidium iodide (PI) analysis of DNA content measured by flow cytometry. (D) Experiments performed as in Fig. 1A with HIRA depletion or (E) CAF-1 depletion. All experiments are

in HeLa cells. All results were obtained at least three independent times, and representative results are shown. See also Figure S2.

Author Manuscript Author Manuscript Author Manuscript Author Manuscript

Author Manuscript Author Manuscript Author Manuscript Author Manuscript

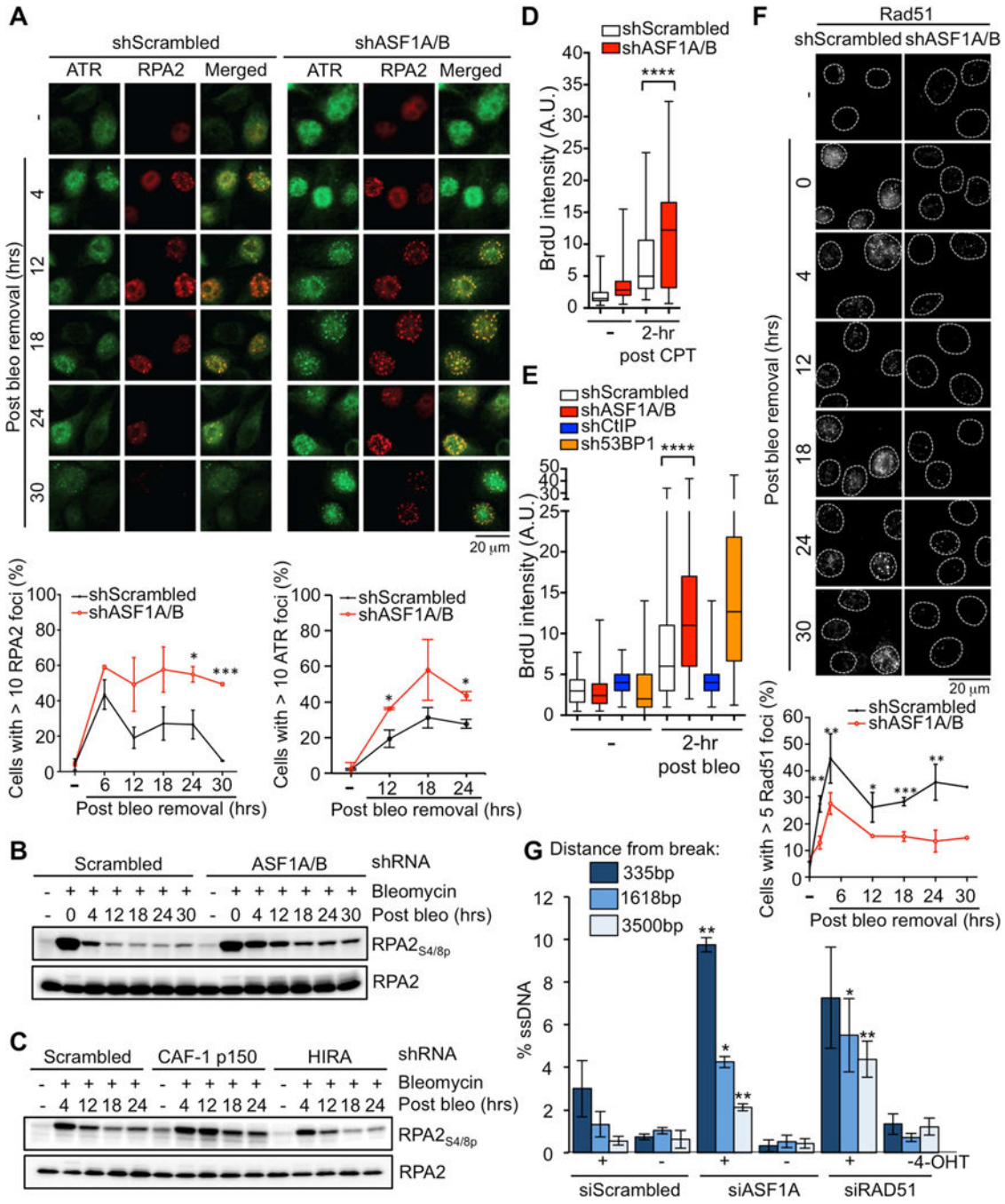

Figure 3. ASF1 is required for the efficient replacement of RPA with Rad51 and preventing excessive end resection

(A) Cells were treated as described in Fig. 1A, followed by immunofluorescence analysis for RPA2 and ATR. The average and standard deviation percent of cells with more than 10 foci, for > 100 cells from three independent experiments are plotted. (B) Performed as described in Fig. 1A. (C) Robust RPA2 phosphorylation in CAF-1 depleted cells, but not HIRA depleted cells, following DSB damage. (D) Accumulation of ssDNA as measured by BrdU fluorescence of undenatured DNA nucleus is depicted by box-and-whisker plot showing medians of n >100, 25th-75th percentiles (boxes) and overall ranges following treatment with

Author Manuscript Author Manuscript Author Manuscript Author Manuscript

5 μM of camptothecin for 2 hours. Student's t-test: ****P < 0.0001. (E) as in (D) but following bleomycin treatment. (F) Cells were treated as described in Fig. 1A followed by immunofluorescence analysis for Rad51. Dashed outlines represent nuclei based on DAPI staining. The average and standard deviation from three independent experiments is shown. (G) Resection around a 4-OHT induced AsiSI site at the indicated distances from the DSB. The average and standard deviation from three independent experiments is shown. Student's t-test: *P < 0.05 **P < 0.01. All results were obtained at least three independent times, and representative results are shown.

Author Manuscript Author Manuscript Author Manuscript Author Manuscript

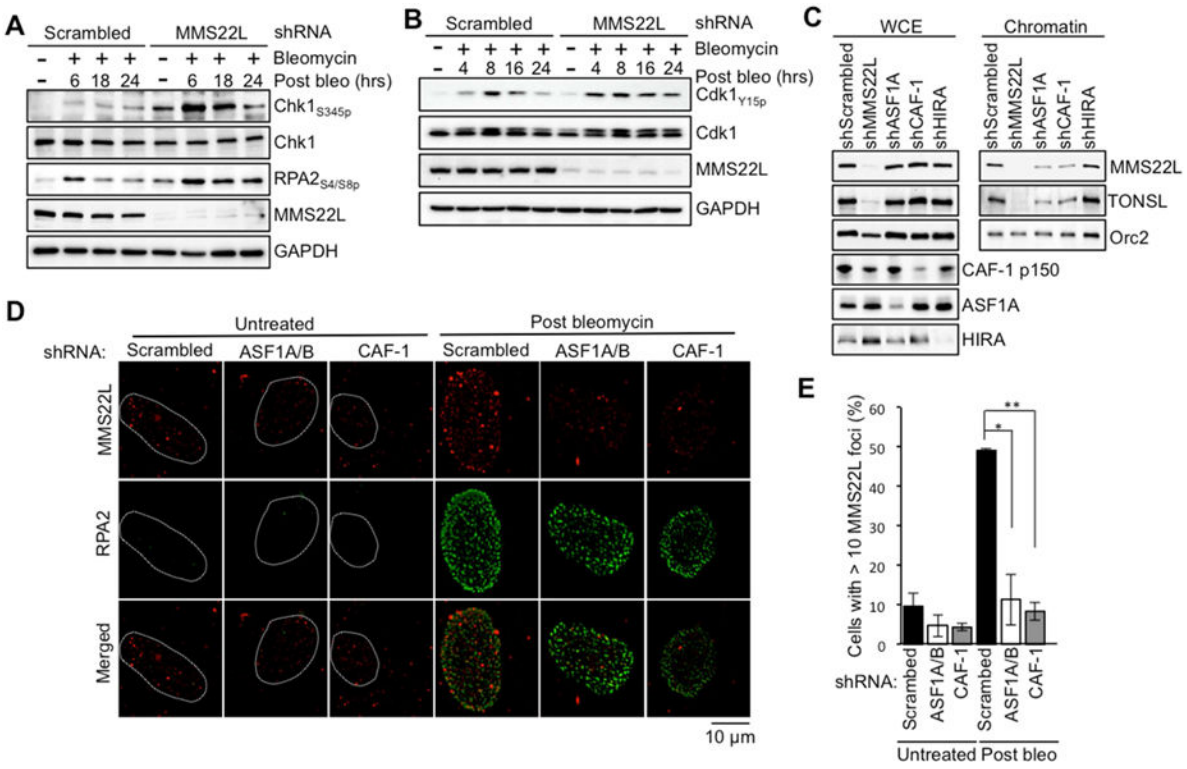

Figure 4. ASF1 and CAF-1 promote MMS22L-TONSL recruitment

(A) DNA damage-induced hyper-phosphorylation of Chk1 and RPA2 (A) and Cdk1 (B) following MMS22L depletion. The experiment was performed as described in Fig. 1–3 but with depletion of MMS22L. (C) Level of TONSL-MMS22L complex in chromatin upon histone chaperone knockdowns. (D) Knockdown of ASF1A/B and CAF-1 leads to reduced recruitment of MMS22L to DNA repair foci. (E) Quantitation of (D). The average and standard deviation from three independent experiments is shown. Student's t-test: *P < 0.05 **P < 0.01. All results were obtained at least three independent times, and representative results are shown. See also Figures S3 and S4.

Author Manuscript
Author Manuscript
Author Manuscript
Author Manuscript

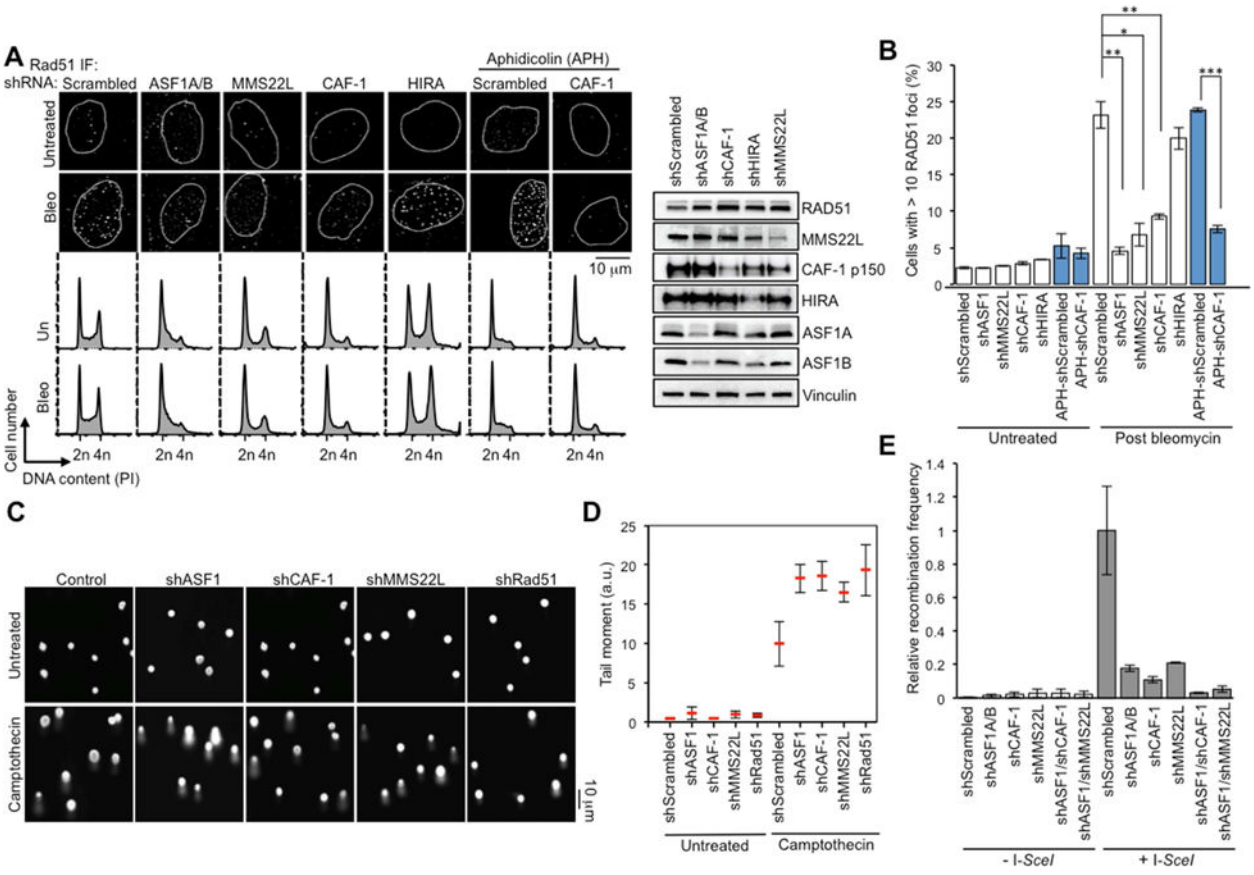

Figure 5. ASF1 and CAF-1 promote Rad51 loading and HR repair

(A) Rad51 foci formation and DNA content in U20S cells with the indicated treatments and knockdowns, using set #2 of shRNAs with westerns showing knockdown efficiency. (B). The average and standard deviation plotted from three independent experiments, with over 100 cells per sample per experiment is shown. Student's t-test: *P < 0.05 **P < 0.01 ***P < 0.001. (C) K562 cells were incubated with 10 μM CPT for 2 hours. (D) quantitation of (C) for > 60 cells per each sample. The red line represents the mean tail moment; error bars were obtained from two individual experiments. (E) The frequency of GFP-positive cells measured by flow cytometry at the indicated times after I-SceI transduction in DR-GFP U2-OS cells is shown. Error bars indicate S.E.M.; n=3. t-test: *P < 0.05 **P < 0.01. All results were obtained at least three independent times, and representative results are shown. See also Figure S5.

Author Manuscript Author Manuscript Author Manuscript Author Manuscript

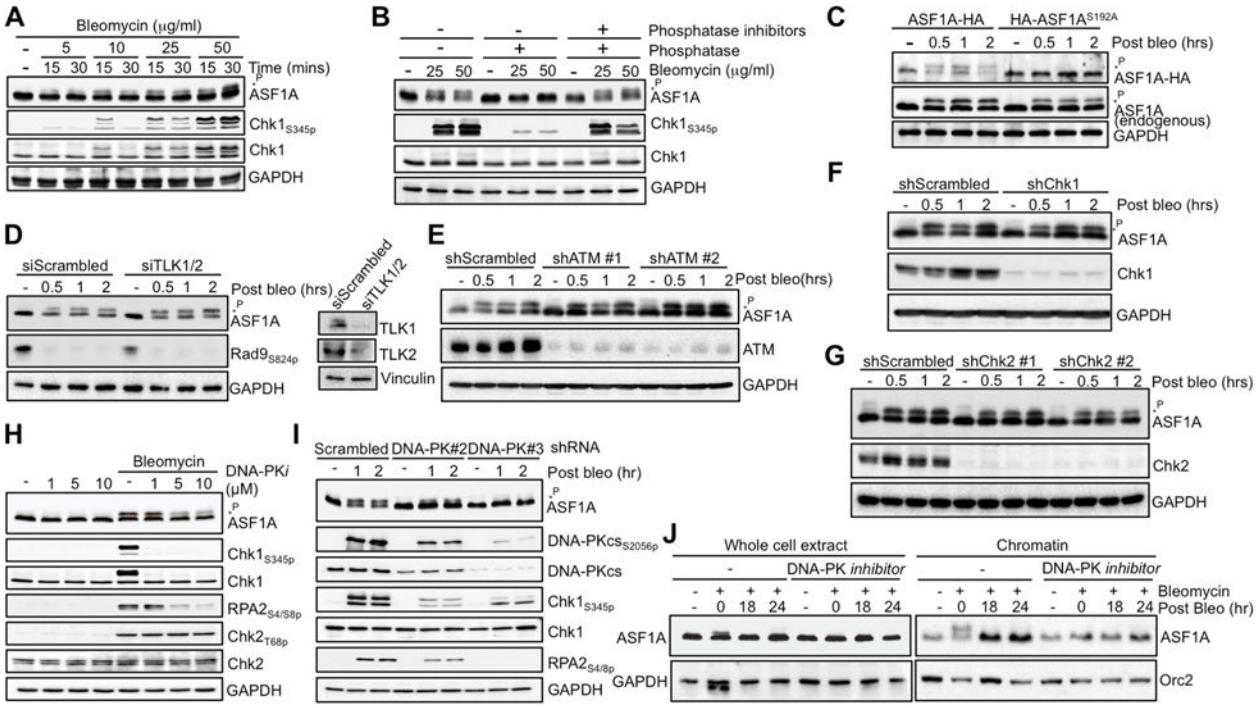

Figure 6. DNA-PK dependent DSB induced ASF1A phosphorylation

(A) HeLa cells were treated with increasing concentrations of bleomycin for 15 and 30 minutes. *p indicates ASF1A phosphorylation. (B). Lysates from cells treated with or without bleomycin were subject to either alkaline phosphatase (NEB) alone or a combination of phosphatase and PhosSTOP phosphatase inhibitor cocktail (Roche) at room temperature for 10 minutes followed by Western blotting analysis. (C) Western blot analysis of ASF1A phosphorylation in cells transiently expressing either C-terminal HA-tagged ASF1A wild type or S192A construct for 24 hours. (D). siRNA of TLK1/2 followed by western analysis of the indicated proteins. (E) as in (D) for ATM knockdown with two different shRNAs. (F) as in (D) for Chk1 knockdown. (G) as in (D) for Chk1 knockdown. (H) as in (D) using DNA-PK inhibitor NU7026. (I) as in (D) upon DNA-PK knockdown. (J) Chromatin extraction using the DNA-PK inhibitor. All results were obtained at least three independent times, and representative results are shown. See also Figure S6.

Author Manuscript Author Manuscript Author Manuscript Author Manuscript

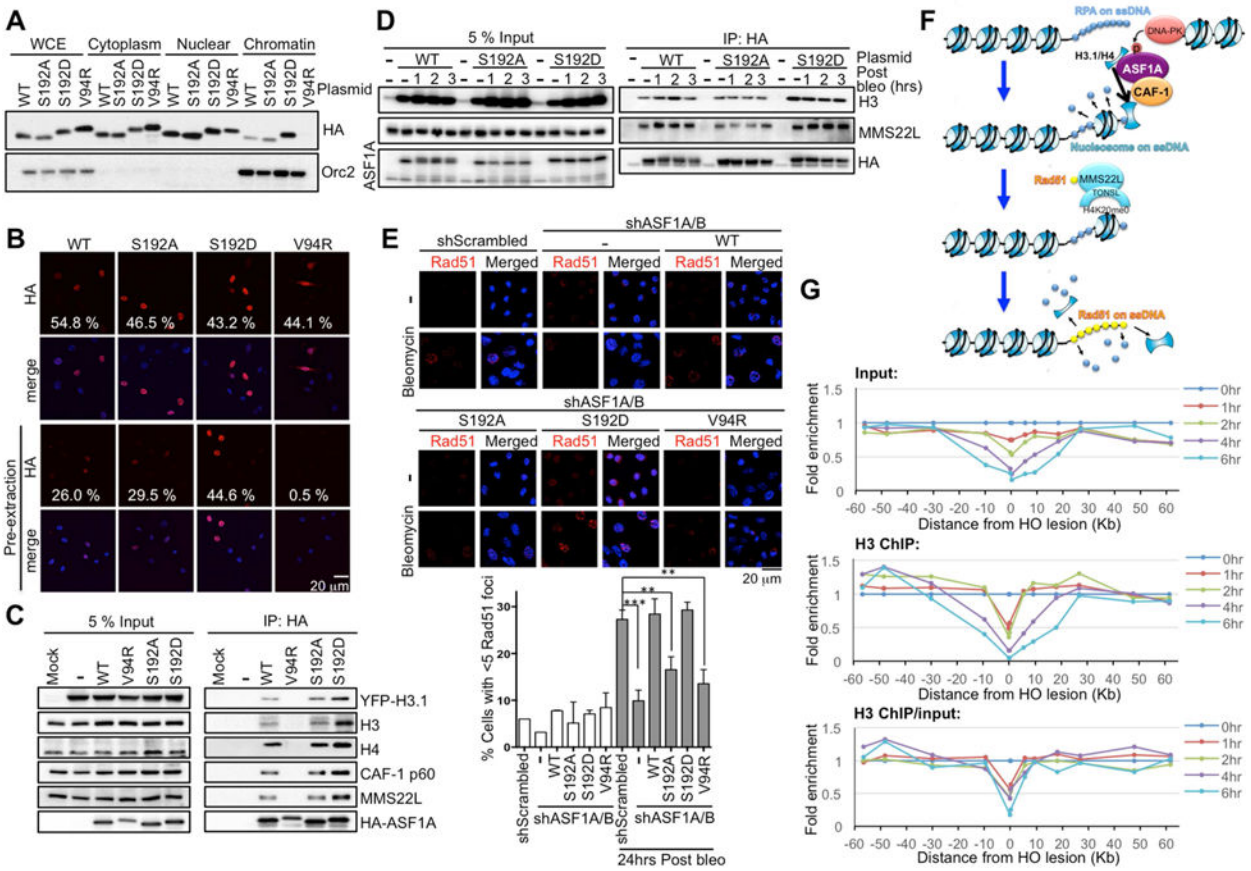

Figure 7. ASF1A phosphorylation promotes Rad51 loading, model and histones loaded onto ssDNA

(A) HA-tagged wild type and mutant ASF1A proteins were transiently expressed in HeLa cells and fractionated into whole cell extract (WCE), cytoplasmic (Cyto), nuclear (Nuc) and chromatin fractions. Orc2 serves as a chromatin bound control. (B) Cells with transient wild type or mutant ASF1A expression were either subject pre-extraction with 0.1% Triton X-100, or not. 100 cells per sample were counted from two independent experiments to determine the percentage of cells with detectable levels of HA-ASF1. (C). HeLa cells with wild type or mutant ASF1A expression were co-transfected with YFP tagged H3.1 for 24 hours, followed by immunoprecipitation analysis. “Mock” received no plasmid. (D) Immunoprecipitation analysis after bleomycin treatment. Samples with double “−“labelling were “untreated”. (E) ASF1A/B depleted cells were transfected with shRNA-resistant HA tagged wild type and mutant ASF1A plasmids and analysed for Rad51 foci. Over 100 cells per sample per experiment were analysed. The average and standard deviation from three individual experiments are shown. Student’s t-test: **P < 0.01 ***P < 0.001. (F) Model described in the text. (G) ChIP analysis of H3 around an HO lesion in a strain lacking donor sequences. All data are normalized to a region elsewhere. All results were obtained at least three independent times, and representative results are shown. See also Figure S7.